Article

Applying Close Range Non-Destructive Techniques for the Detection of Conservation Problems in Rock-Carved Cultural Heritage Sites

William Frodella [1,2,*], Mikheil Elashvili [3], Daniele Spizzichino [4], Giovanni Gigli [1,2], Akaki Nadaraia [3], Giorgi Kirkitadze [3], Luka Adikashvili [3], Claudio Margottini [2], Nikoloz Antidze [5] and Nicola Casagli [1,2]

[1] Earth Science Department, University of Florence, Via G. La Pira 4, 50121 Florence, Italy;
giovanni.gigli@unifi.it (G.G.); nicola.casagli@unifi.it (N.C.)
[2] UNESCO Chair on Prevention and Sustainable Management of Geo-Hydrological Hazards,
University of Florence, Largo Fermi 1, 50142 Florence, Italy; claudio.margottini@unifi.it
[3] Faculty of Natural Sciences and Engineering, Ilia State University, Kakutsa Ave 3/5, 0162 Tblisi, Georgia;
mikheil_elashvili@iliauni.edu.ge (M.E.); akaki.nadaraia.1@iliauni.edu.ge (A.N.);
giorgi.kirkitadze.3@iliauni.edu.ge (G.K.); luka.adikashvili.1@iliauni.edu.ge (L.A.)
[4] Institute for Environmental Protection and Research (ISPRA), ia V. Brancati 48, 00144 Rome, Italy;
daniele.spizzichino@isprambiente.it
[5] Georgian the National Agency for Cultural Heritage Preservation of Georgia (NACHPG), 27 Atoneli Street,
0105 Tbilisi, Georgia; info@heritagesites.ge
* Correspondence: william.frodella@unifi.it; Tel.: +39-055-275-5979

Abstract: Rock-carved cultural heritage sites are often developed in slopes formed by weak rocks, which due to their peculiar lithological, geotechnical, and morpho-structural features are characterized by excellent carvability, which at the same time makes them prone to weathering, deterioration, and slope instability issues. In this context the use of advanced close-range nondestructive techniques, such as Infrared Thermography (IRT) and Unmanned Aerial vehicle-based Digital Photogrammetry (UAV-DP) can be profitably used for the rapid detection of conservation issues (e.g., open fractures, unstable ledges-niches, water seepage and moisture) that can lead to slope instability phenomena. These techniques, when combined with traditional methods (e.g., field surveys, laboratory analysis), can provide fundamental data (such as 3D maps of the kinematic mechanisms) to implement a site-specific and interdisciplinary approach for the sustainable protection and conservation of such fragile cultural heritage sites. In this paper some examples of conservation problems in several rupestrian sites characterized by different geological contexts, from the mountainous regions of Georgia to the ancient city of Petra in Jordan, are presented, with the aim of evaluating the potential of the proposed integrated approach. The final aim is to provide conservators, practitioners, and local authorities with a useful, versatile, and low-cost methodology, to be profitably used in the protection and conservation strategies of rock-carved sites.

Keywords: infrared thermography; UAV digital photogrammetry; cultural heritage; landslides; conservation issues

1. Introduction

Rock-carved settlements were among the first man-made works in the history of humanity, therefore representing the roots of human society [1]. These sites are not always in equilibrium with the environment, since they are continuously impacted and weathered by several internal and external factors, both natural and human-induced, with rapid and/or slow onset [2]. These factors include major sudden natural hazards, such as earthquakes or extreme meteorological events but also slow, cumulative processes such the erosion of rocks, compounded by the effect of climate change, without disregarding the role of humans, especially in conflict situations [3]. Rock-carved cultural heritage sites were often

excavated in steep slopes formed by so-called "weak rocks" (e.g., soft sandstones and tuffs characterized by low compressive strength values), which give the advantage of an excellent carvability but on the other hand are affected by major conservation issues in the field of rock slope stability and rock weathering [4]. The peculiar lithological and geotechnical features of these rocks (highly heterogeneous fabric with abundant clayey matrix, high porosity and low compressive strength), together with the natural morphological and structural setting of the excavated slopes (e.g., open fractures, presence of ledges-niches) and the presence of anthropic carved structures (caves, chambers and corridors), make these sites particularly fragile and prone to weathering, erosion, and slope instability processes [5,6]. In this context a further element of damage is represented by moisture expansion, caused by water runoff and groundwater, which reduces the rock uniaxial compressive strength (UCS) [7–9]. The discontinuity pattern also controls the structural stability of slopes, since their geometry with respect to the slope face can determine different kinematic behavior of the rock mass, while their engineering properties are adversely affected by water seepage and moisture, which in turn causes weathering and discoloration films, therefore reducing the wall strength [10,11]. Chemical weathering in particular, leads to the eventual decomposition of silicate minerals to clayey minerals, leading to the loosening of the rock mass and the widening of the joints creating potential instabilities such as open features [12]. Furthermore, the rockmass discontinuity networks are areas of preferential of rainfall infiltration and seepage, enhancing concentrated erosion [13]. In sandstone material in particular, the weathering processes due to the presence of water (e.g., arenitization, crust formation, peeling, decohesion, detachment, exfoliation, and biodeterioration) usually show one-directional water circulation from the outside to inside, with the prevalence of surface moisturizing and rapid evaporation, causing an increase in porosity, which further facilitates water infiltration [14,15]. The combination of the above-mentioned processes causes deterioration and structural instability of the rock-carved settlements as well as landslide processes, representing serious constraints to the future conservation of the sites and to the safety of the visitors [16,17]. Nowadays these sites represent unique cultural heritage sites, often included in the UNESCO World Heritage [18] or Tentative lists [19] which are visited daily by thousands of visitors. This is a resource for the local economies, but at the same time represents both an element of anthropic pressure in a fragile system between natural and ancient cultural elements, and a risk increasing factor. Therefore, the protection and conservation of rock-carved sites are pressing issues not only for the community of conservators, practitioners, and scientists but for the whole society. For an effective and sustainable conservation strategy it is necessary to implement a complex and specific interdisciplinary approach, that should be planned involving nondestructive techniques and consider in turns, the site characteristics (topography, geomorphological-geological setting) and typology of the related hazard [20–22]. In this perspective the use of close-range remote sensing (RS) techniques, such as terrestrial infrared thermography (IRT) and Unmanned Aerial vehicle-based Digital Photogrammetry digital photogrammetry (UAV-DP), represent effective tools for surveying rupestrian environments for slope morpho-structural characterization and detection of criticalities (e.g., weathering, erosion, slope instabilities), since they allow for fast, cost-effective, and easily updatable acquisitions over wide and inaccessible areas. RS techniques offer clear advantages with respect to traditional methods, by optimizing field work and granting the safety of both the operators and the monument [23,24]. On the other hand, traditional methods are still fundamental in order to gather rock geotechnical parameters and validate the outcomes of the remotely sensed data. Rock-carved monuments of Georgia represent a unique cultural heritage: ancient cities, churches and monastery complexes carved in rock, painted and decorated by hermit monks, form a remarkable junction between architectural monument and unique natural-geological landscapes, having their roots deep in the history of Georgian state [25] (Figure 1).
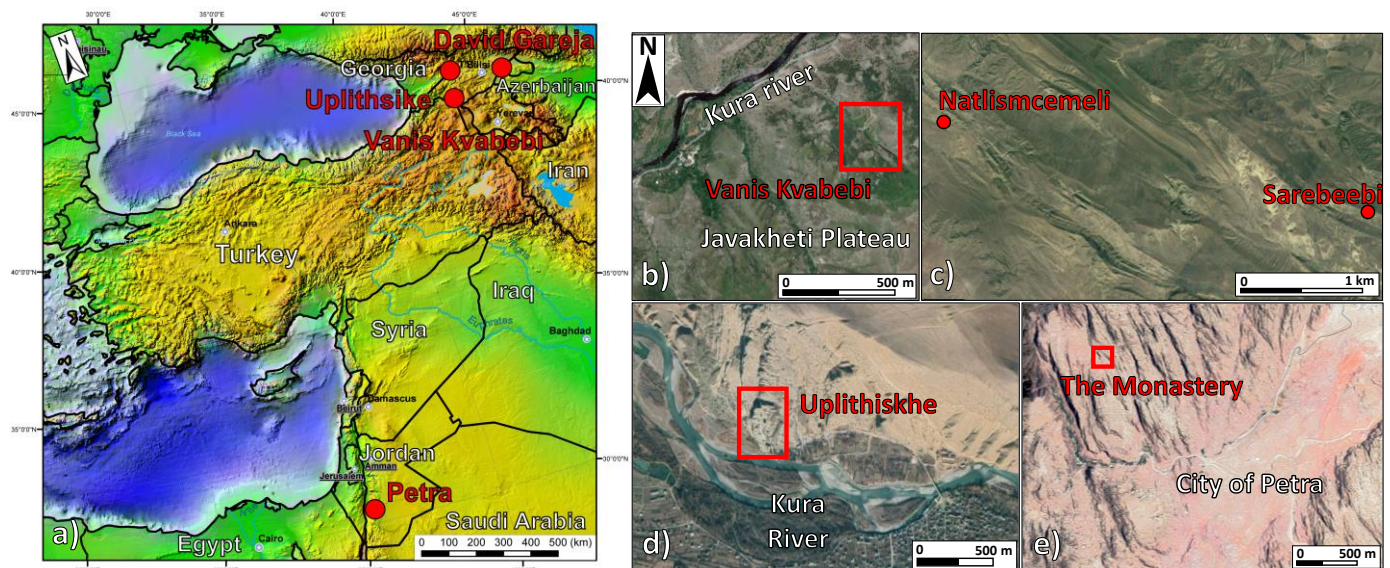
Figure 1. Map with the location of the analyzed rock-carved cultural heritage sites (**a**); locations at a higher scale: Vanis Kvabebi (**b**); David Gareja area (**c**); Uplistsikhe (**d**); The Monastery of Petra (**e**).

Often carved in weak rocks such as volcanic tuffs and soft sandstones, these sites are particularly vulnerable to weathering, erosion, and slope instability phenomena and are therefore often inscribed in the UNESCO Tentative List. In recent years, these sites have been undergoing a multidisciplinary research activity coordinated by the Georgian National Agency for Cultural Heritage Preservation of Georgia (NACHPG), with the support of a team of Georgian and international experts, in order to implement an extensive site-specific protection and conservation strategies [11,13,20,23]. Arguably one of the most iconic monuments of the Petra Archaeological Park in Jordan, World Heritage site since 1985, Al Deir (also called "the Monastery") [26], is affected by seepage phenomena leading to salt damage processes, one of the main factors of weathering and erosion of the famous red sandstones of Petra (Figure 1).

This work shows several applications of close-range remote sensing techniques combined with traditional methods (e.g., field surveys, laboratory analysis) for the detection and analysis of slope instabilities and conservation issues. In detail, IRT and UAV-DP were integrated with traditional field surveys and geotechnical laboratory analyses, with the aim of performing a morphological, geostructural-geomechanical characterization and 2D-3D kinematic analysis of several cultural heritage sites carved in rock masses (Vanis Kvabebi, David Gareja and Uplistsikhe in Georgia, the monastery of Petra in Jordan). The final aim was to provide the basic knowledge on the acting instability and degradation/weathering processes, to detect the main conservation criticalities to provide suggestions for the planning and implementation of mitigation strategies. Results demonstrate that the applied methodology can provide fundamental data to implement a site-specific and interdisciplinary approach for the sustainable protection and conservation of rock-carved cultural heritage sites, also showing suggestions for management plans in sites characterized by similar engineering geological issues.

2. Case Studies Geological-Historical Background and Conservation Problems

2.1. Vanis Kvabebi

The monastery complex of Vanis Kvabebi is in southwestern Georgia in Samtskhe-Javakheti volcanic highland of the Lesser Caucasus (Figures 1a,b and 2). It is carved in the volcanic steep slopes of the Kura river gorge right bank, where the Javakheti plateau develops [27,28].
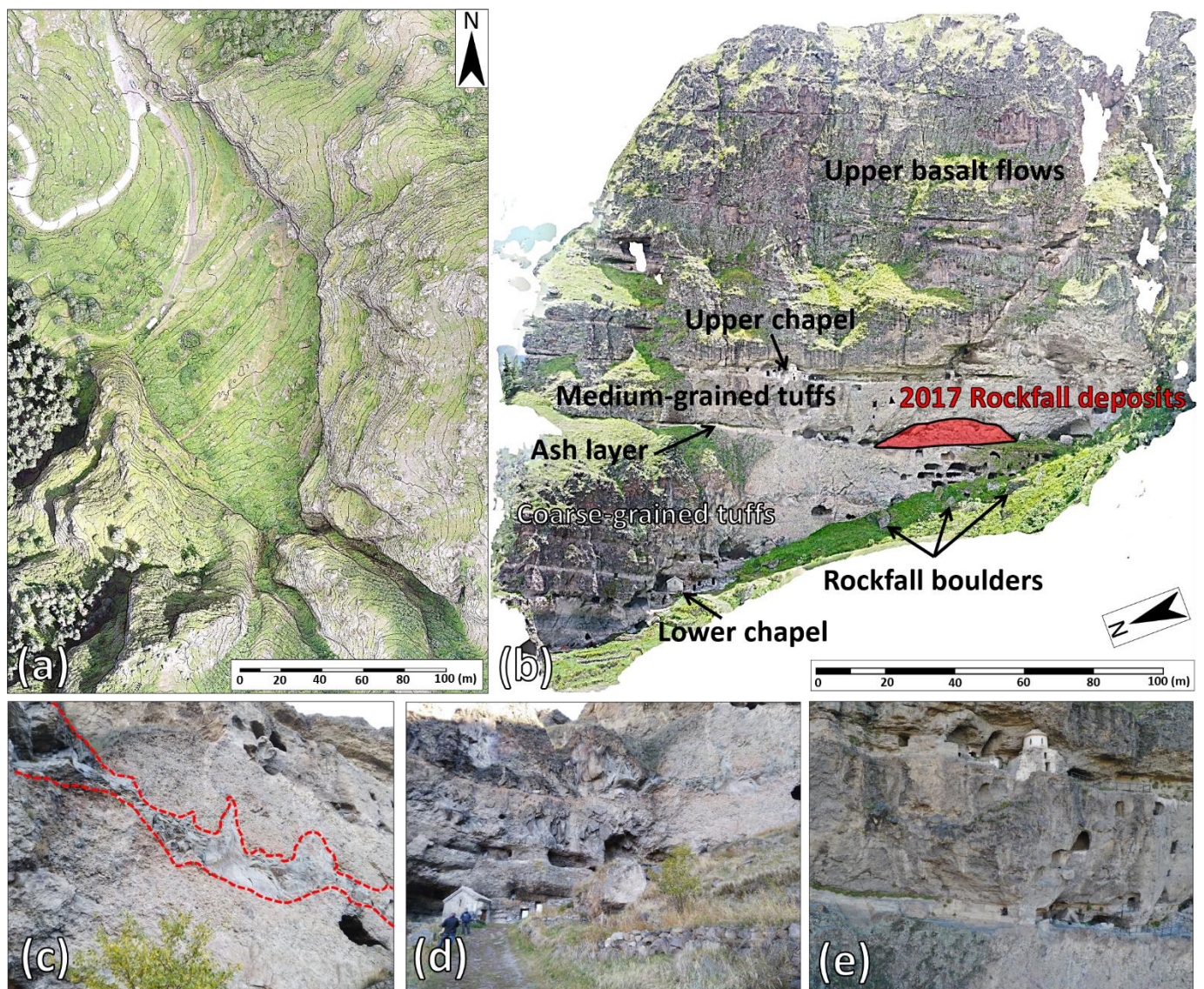
Figure 2. Vanis Kvabebi geological-geomorphological features: true color UAV-DP photogrammetric digital models: nadiral view (**a**); frontal view of the eastern main cliff of the monastery showing the outcropping lithologies of the Godertzi formation and the 2017 rock fall deposits (**b**); welded tuffs (dashed red line) (**c**); lower chapel with ancient rockfall boulder (**d**); upper chapel (**e**).

From a geomorphological point of view the site develops in a V-shaped ravine NW oriented, bounded by subvertical cliffs, up to 200 m in height (Figure 2a,b). From a geologic point of view the study area is characterized by the Godertzi formation (from Upper Miocene to Lower Pliocene in age), which is formed by an upper section of andesitic, dacitic, and rhyodacitic lava flows, with rare occurrence of basaltic rocks (about 600–700 m in thickness), and a lower section of pyroclastic deposits such as volcanic breccias and tuffs of different granulometry, with andesitic-dacitic composition (200–250 m in thickness) [29,30]. On top of the Goderdzi formation lies discordantly the Akhalkalaki suite: a thick series of dolerites and basalts of Quaternary age [31]. Along the cliff of the monastery the upper portion of the Godertzi formation is widely exposed, formed from bottom to top by a layer of coarse-grained tuffs (over 30 m in thickness), followed by a 2–3.5 m thick volcanic andesitic ash layer and an upper level of medium-grained tuffs (about 20 m thick), including welded tuffs [31,32]; the basalt flows the of the Akhalkalaki suite overlie the former (Figure 2b). Far less studied with respect to the site of Vardzia, just 2 km to the

NW [13], Vanis Kvabebi is a cave monastery dating from 8th century, consisting of a maze of tunnels and caves running on 19 levels (Figure 2b).

The monastery consists also of a defensive wall system built in 1204 and two chapels: a newer stone church (still inhabited nowadays by monks) near the top of the defensive wall (Figure 2d), and a smaller, domed church that clings to the rock on the level of the highest tunnels (Figure 2e). Two levels of pathways are carved in the rock to connect the various levels. Due to its peculiar litho-stratigraphic, structural, and morphological setting the site is undergoing weathering and degradation processes which trigger instability mechanisms, testified by ancient rock fall deposits constituted by large boulders lying at the bottom of the ravine (Figure 2b). In 2017 a rock fall impacted a touristic pathway enhancing the need for detailed multidisciplinary studies to plan a surveying-monitoring strategy and implement a management plan for the protection-conservation of the site and a safe touristic access. Since 2018 Vanis Kvabebi has been undergoing an intensive campaign of protection and restoration activities, involving remote surveying and field activities for preliminary landslide hazard assessment for the planning of mitigation measures.

2.2. David Gareja

The David Gareja monastery complex is located in Kakheti semidesert region (Eastern Georgia), about 25 km southeast of Tbilisi (Figures 1a–c and 3). From a geological point of view the area is formed by a thick sequence of soft sedimentary rocks (Lower Miocene to Pliocene in age) characterized by a monocline "hogback type" structure, with strata dipping SW with low-gentle angles (Figure 3a), from very coarse-grained, pebbly thick-bedded sandstones to coarse-grained soft sandstones, siltstones, and clays (Figure 3b,c) [24]. In detail, the stratigraphic sequence is formed by: (i) lower Miocene sandy clays, dark-brown and brownish-gray clays with interbedded sandstones, and rare conglomerate interlayers; (ii) upper Miocene is represented mostly by shallow and coastal sediments, but there are also deep-sea sediments represented by yellowish-gray calcareous sandstones; (iii) Pliocene sediments are represented by continental and marine facies consisting of coarse-grained yellowish-gray sandstones with numerous small pebbles and thick basal conglomerates with volcanic ash interbeds [33,34].

David Gareja is one of the most important landmarks of Georgia and is characterized by a unique combination of historic architecture and peculiar geological/geomorphological features, representing a remarkable example of harmonious interaction of man-made structures with a dramatic landscape. Part of the UNESCO Tentative List since 2007, it includes the complex of 19 medieval monasteries with approximately 5000 cells for monks [35]. Some mural paintings preserved in the cave monasteries (the oldest of which go back to the 6th–8th century), are considered a masterpiece of Georgian medieval art as they contain the portraits of Georgian kings (Figure 3a,b). In medieval times David Gareja served as one of the most important monastic and pilgrimage centers of Georgia. The Mongol invasions of the first half of the 13th century brought monastic life to an end. New mural paintings were not to be made until the 17th and 18th centuries, when serious attempts were made to revive monastic life. The life of the monasteries ended again in 1921 during the Soviet period, when the monasteries were closed, and some sites used in later years for artillery practice [25]. Within the whole complex the most important monasteries (still inhabited today by monks) are St. David Laura Monastery (Lavra), John the Baptist (Natlismcemeni), and the Virgin (Dodos Rka). The rest of the 16 monasteries (amongst which Sabereebi represents an important example) are currently abandoned.
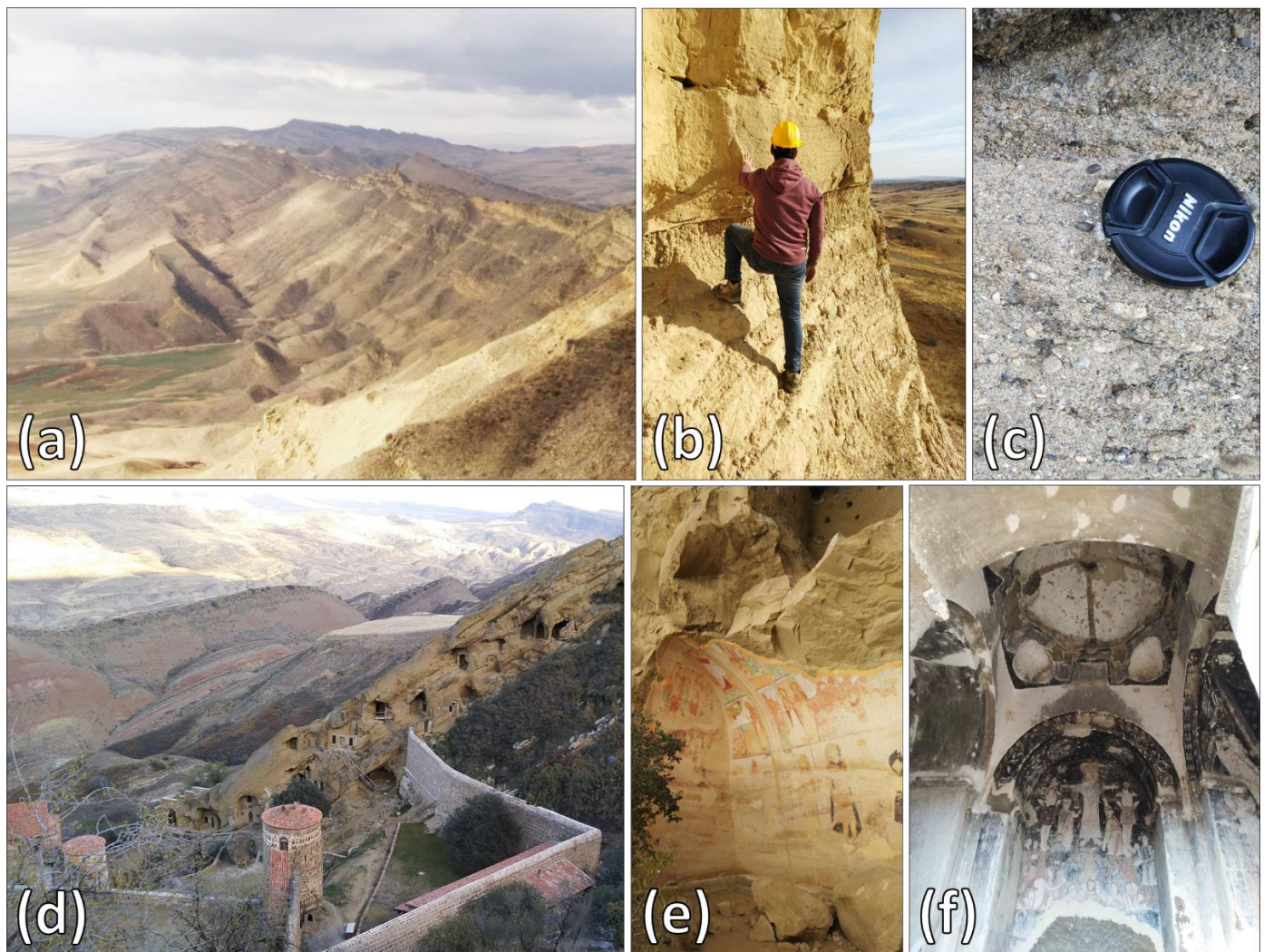
Figure 3. The David Gareja area: structural monocline (**a**); outcropping lithologies (silts and clays with thick sand layer (**b**) coarse-grained sands-conglomerates (**c**); Lavra monastery (**d**); Examples of frescoed cave chapels in the monasteries of Udabno (**e**) and Sabereebi (**f**).

2.3. Uplistsikhe

Uplistsikhe ("the lord's fortress" in Georgian) is an ancient cave town-fortress in eastern Georgia about 50 km NW of Tblisi (Figures 1a–d and 4). From a morphological point of view the Uplistsikhe complex is located on the left bank of the Kura River on the slopes of the Kvernaqi Range. In detail, the site develops on top of a rocky terrace bordered to the south-west by a rock cliff up to 40 m high and is completely carved into a thick sequence of Upper Oligocene to lower Miocene quartz coarse sandstones, gently dipping towards SE (Figure 4a,c) [36]. Being carved on the top of the rock strata in an open space of over 8 ha, the site is quite different from most other rupestrian monuments of Georgia, which instead are carved in near vertical cliffs. The uniqueness of Uplistsikhe is represented by a multilevel archaeological-architectural site with structures dating from the early Iron Age up to the late medieval period and is notable for the unique combination of various styles of rock-cut cultures from Anatolia and Iran, as well as the coexistence of pagan and Christian architecture [37].

Figure 4. The Uplistsikhe cave town complex: top of the rocky terrace with the brick church (**a**); examples of cave systems and defensive walls (**b**); the unstable rock cliff bordering the site (red dashed circles highlight April 2019 detachments, Areas 1–2, the black circle the one from July 2019, Area 3) (**c**); examples of sandstone wind weathering (corrasion) (**d**).

Considered as one of the oldest urban settlements in Georgia and an important political, cultural, and religious center, it flourished during Hellenistic and Roman times, while its decline started in the 4th century. It then acted as a stronghold during the Muslim conquest in the 8th–10th centuries, while the Mongol raids in the 14th century marked the ultimate eclipse of the town, after which the town was abandoned. It consists of a defensive wall, a ditch, streets, tunnels, water pipes, and drainage channels carved in rock. At the summit of the complex a Christian church was built in the 6th century (Figure 4a,b). The current morphology of the site is the result of active tectonics (several parts of the most vulnerable areas were destroyed by an earthquake in 1920), weathering and erosion due to water infiltration and runoff (also caused by the Kura river action), and wind erosion. In this context ancient rockfall deposits at the slope-toe show that slope instability phenomena have contributed to the shaping of the cliff (recent minor rockfalls were reported from June 2018 to October 2019). This led NACHPG to start a conservation program in 2000 [38], while in 2007 the whole complex was enlisted in the tentative list for inclusion into the UNESCO World Heritage program [39].

2.4. The Monastery of Petra

The monastery is located high in the hills northwest of the center of the ancient city of Petra (Figures 1a–e and 5). From a geological point of view the area is characterized by the Upper Umm-Ishrin red-pink massive quartzose subarkosic sandstone, middle to late Cambrian in age [40] (Figure 5a). The monastery is a monumental building carved out of rock in the typical red sandstone of Petra, dating to the mid-first century CE. The huge façade and the inner chambers probably originally served a complex religious purpose and were possibly used as a church in the Byzantine period [41]. In April 2011, an important seepage coming from several points on the rock wall to the left side of the monument were detected [42], also extending towards the base of the monument (Figure 5b,c). This seepage caused a widespread salt damage process on the monument surface determining serious constraints for the conservation of the monument. This process when combined with wind action, as well as the harsh daily excursions of temperature and relative humidity, are the main factors of weathering and erosion of the famous red sandstones of Petra (Figure 5). In fact, most of Petra's monuments have deteriorated at a fast pace over recent years [43];

for this reason, in 1998 the World Monument Fund included Petra in the list of the one hundred most endangered monuments in the world [44].
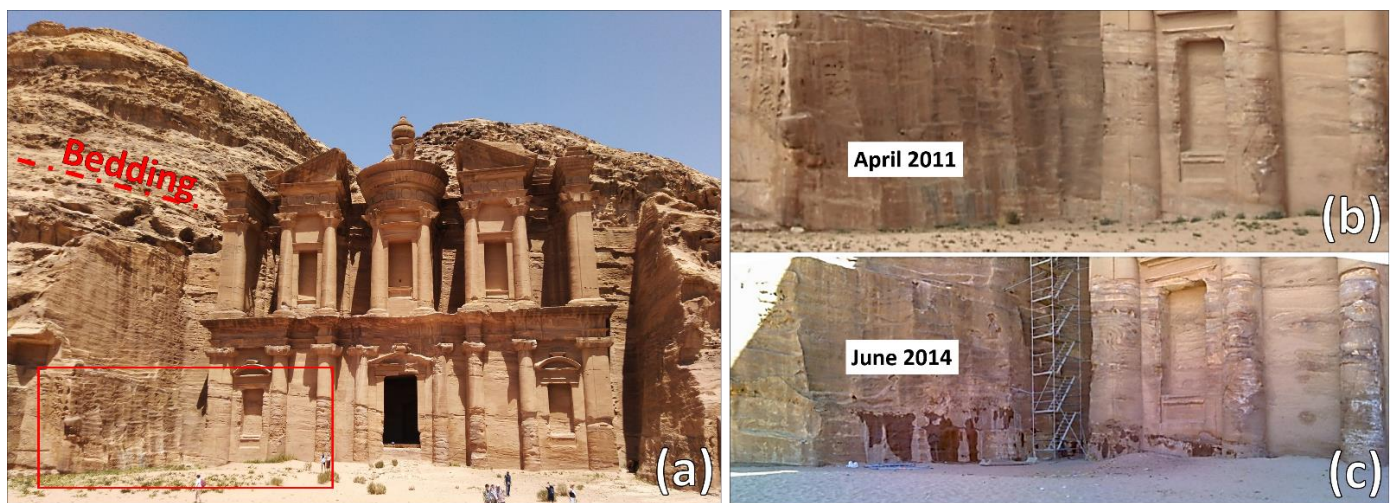
Figure 5. The Monastery of Petra: rock mass on the right side of the monument showing the area of interest (red rectangle) and bedding of the sandstones (**a**); pictures of the area of interest during the surveys of April 2011 (**b**) and June 2014 (**c**).

3. Materials and Methods

During the second half of 2018 field inspection, IRT and UAV-DP surveys were carried out in the areas of Vanis Kavbebi, David Gareja, and Uplithsike [24,36]. IRT analysis was aimed at detecting conservation problems and integrating the field surveys in the geomechanical characterization of the rock slopes (with special regards to fracture opening and seepage). UAV-DP was used to obtain high resolution 3D models, to be used as a detailed topographic base, perform the modelling of the drainage network and the 3D kinematic analysis. In Petra in June 2014 field surveys and IRT inspections were carried out in the framework of the integrated management plan of Petra archaeological park to investigating the hydrogeological setting of the monastery sector of rockmass.

3.1. Field Surveys and Geotechnical Analysis

Field surveys were aimed at identifying stratigraphic and structural elements representing predisposing factors for slope instability phenomena. Traditional geostructural data were collected and analyzed with RocScience Dips © software [45] in order to detect the bedding planes and the main sets of discontinuities, to be used as input data for both the 2D and 3D kinematic analysis. Rock samples were collected in the field during a scientific mission conducted in Georgia in November 2018. A preliminary set of laboratory analyses were aimed at assessing the main physical and mechanical parameters, to be used in further detailed stability modelling. The rock samples were analyzed in order to detect main physical and mechanical parameters. The following laboratory tests were conducted according to [46]: (1) tilt test, (2) point load test, (3) real unit weight (hydrostatic weighing). Since many samples were easily broken even by touch, some tests (especially those in water immersion) were not carried out.

3.2. IRT Surveys

InfraRed Thermography (IRT) is a nondestructive diagnostic technique capable of remotely mapping the investigated scenario's surface temperature [47]. It can provide detection of subsurface defects on wide areas, to be used as an alternative or complement to conventional inspection technologies in a wide variety of scientific applications [48]. IRT is accomplished by means of Infrared (IR) calibrated cameras (thermal cameras), capable of detecting the thermal radiation. The product of an IRT survey is a digital image acquired by the thermal camera array detector (called "thermogram" or "thermographic image"),

which following the correction of the sensitive parameters (such as object emissivity, path length, air temperature, and humidity) is converted by the camera's built-in processor to a surface temperature map of the investigated scenarios [49]. During recent decades, thanks to the technological development of portable high resolution and cost-effective thermal imaging cameras, IRT has been widely used in the field of civil engineering and cultural heritage for the detection of structural damages, water seepage, plaster detachments, moisture, and surface weathering on different materials (stone, concrete, masonry) [50–54] but rarely in rupestrian sites [13,24]. In the analysis of slope instability phenomena, IRT can lead to the detection of irregular thermal patterns (thermal anomalies) which can reveal the presence of potential criticalities such as: (i) open fractures; (ii) moisture or seepage zones; (iii) ledge-niche systems; (iv) cavities; (v) lava flows [13,47,55–59]. The surveys were performed in hand-held mode using thermal cameras with a focal plane array (FPA) microbolometer sensor [60,61]. The surveying parameters of the sites are reported in Table 1. Thermographic image correction, thermal focusing, mosaicking, and histogram equalization were performed by means of FLIR Tools+ software [62]. ESRI ArcMap package was also used to create classified surface temperature maps using quantile function [63].

Table 1. IRT survey parameters of the analysed sites.

Case Study	Thermal Camera	Camera Resolution (pix)	Field of View (°)	Survey Period	Slope Aspect	Sensor-Target Distance (m)	Image Resolution (cm)	Air Temperature (C°)— Relative Humidity (%)
Vanis Kvabebi	FLIR SC620	640 × 480	24 × 18	November 2018	W/E	100	6.6	14.4–63.4
Natlismcemeli	FLIR SC620	640 × 480	24 × 18	November 2018	S	110/20	7.1/1.2	13.4–65.9
Sabereebi	FLIR SC620	640 × 480	24 × 18	November 2018	SW	100/20	6.5	22.6–39.8
Uplistsikhe	FLIR SC620	640 × 480	24 × 18	November 2018	SW	100	6.6	21.3–33.6
Petra	FLIR B425	320 × 240	25 × 19	June 2014	SW	20	2.6	26–21

3.3. DSM Creation and Surface Runoff Modelling

Digital photogrammetry (DP) is a well-established technique for efficient and accurate 3D geometric data from stereoscopic overlaps of photo sequences captured by a calibrated digital camera [64]. This technique can provide in a short time high resolution 2D and 3D surfaces, allowing for a detailed and highly accurate representation for the analysis of the geometrical-structural setting [65,66]. In the past few years, thanks to the rapid technological development of digital cameras and low-cost UAV, DP has led to new, promising scenarios in cultural heritage applications [67–69]. UAV-DP and TLS surveys were carried out in Vanis Kvabebi, David Gareja, and Uplistsikhe in 2018, with the aim of obtaining a high resolution orthophoto and a complete 3D digital model of the analyzed rock-cut slopes and buildings part of the cultural heritage sites. Close-range aerial photogrammetric surveys were carried out using DJI Phantom 4Pro and DJI Mavic Pro quadcopters. Both UAVs are equipped with quite similar cameras, including the 3-axis gimbal and image stabilization systems (Table 2).

Table 2. Technical information of the adopted devices and the obtained DSMs resolutions.

Digital Cameras	Sensor Accuracy (″)	Pixels (M)	Field of View (°)	Lens (mm)	Measurement Range (m)
DJI Phantom 4Pro	1	20	84	35	1 m–∞
DJI Mavic Pro 2	1	20	77	28	1 m–∞
Laser Scanner	Accuracy (mm)	Divergence (mrad)	Resolution (arcsec)	Angular step (°)	Measurement range (m)
Z-400	5 mm	0.3	1.8 arcsec	0.0024°–0.288°	1.5–280
Study site DSM-Orthophoto resolution (cm)	**Vanis Kvabebi** (10-5)	**Natlismcemeli** (8-4)	**Sabereebi** (9-4.5)	**Uplistsikhe** (7-3.5)	

Acquisitions were performed using preloaded flight trajectories and controlled overlaps between the images using Pix4Dcapture software. Structure-from-motion (SfM) image processing has been applied, using Agisoft Photoscan software [70]. To achieve high quality of obtained 3D models and precision in georeferencing, ground control points were used with measured absolute coordinates using DGPS (CORS system, with sub-centimeter range horizontal errors in absolute coordinates) or Robotized Total Station devices. Several products of high accuracy were delivered, such as DSM and orthophoto mosaics in both horizontal and vertical projections (Table 2), with sub-decimeter resolution (horizontal errors in a decimeter range). Moreover, high-resolution photo textures allowed for true-colored DSMs and for the visual estimate of the damaging effect of water channels and crack systems of water infiltration. To obtain complete 3D models UAV-DP was integrated with TLS surveys [24,36], which were carried out by means of a long-range 3D terrestrial laser scanner (Riegl VZ-400) [71] (Table 2). ArcMap (ESRI) Hydrology Tools package was applied using Flow Direction, Accumulation and Stream Order functions for the analysis of the slope scale drainage system [63]. This allowed for the modelling of surface water run off trajectories, calculating the corresponding watersheds and categorizing the stream order on the DSMs [13,58].

3.4. Kinematic Analysis

In order to define the main rock slope instability processes, a spatial kinematic analysis can be performed by using discontinuity orientation data, semiautomatically and manually extracted from the obtained slope 3D surface models. Given the slope geometry and the discontinuity orientation, this kind of analysis is capable of mapping the spatial probability of occurrence for the following instability mechanisms:

(i)   plane failure (PF) [72].
(ii)   wedge failure (WF) [72].
(iii)   block toppling (BT) [73].
(iv)   flexural toppling (FT) [73,74].

Ref. [75] introduced a kinematic hazard index for each instability mechanism. These values are calculated by counting poles and discontinuities in the critical areas of the stereographic projection:

(v)   Npf = number of poles satisfying plane failure conditions.
(vi)   Iwf = number of intersections satisfying wedge failure conditions.
(vii)   Nbt = number of poles satisfying block toppling conditions.
(viii) Ibt = number of intersections satisfying block toppling conditions.
(ix)   Nft = number of poles satisfying flexural toppling conditions.

The kinematical hazard index is calculated as follows:

(i)   Cpf = 100 × (Npf/N) for plane failure.
(ii)   Cwf = 100 × (Iwf/I) for wedge failure.
(iii)   Cbt = 100 × (Nbt/N) × (Ibt/I) for block toppling.
(iv)   Cft = 100 × (Nft/N) for flexural toppling.

where N and I are the total number of poles and intersections, respectively.

By using specific software, such as KARS [75], Rock Slope Stability [76], or DiAna-k [77], it is possible to load a great number of discontinuities with different friction angles. Intersection lines are calculated automatically, together with the equivalent friction angle, based on the friction angles of the intersecting planes and the shape of the wedge [75]. The analysis can be performed for specific slope orientations or for each cell of a 3D surface (true 3-D kinematic analysis). This method overcomes many limitations of the traditional approaches, as it is possible to employ true 3D surfaces, and the kinematic conditions leading to the investigated instability mechanisms have been extended to overhanging slopes. Moreover, a global kinematic index (GKI) can be introduced, to quantitatively define the rock instability hazard for each sector of the slope, whatever the effective instability mechanisms. The input data of this method are the high-resolution 3D meshes obtained

from terrestrial laser scanner or photogrammetric surveys and the discontinuities extracted with the manual and semiautomatic [78] methods. As the orientation of fractures is related to the tectonic processes that have been acting in the investigated areas, a kinematic analysis can be useful to highlight the rock wall sectors which are more prone to instability processes. This approach was used for the obtained 3D surfaces using CloudCompare © software [79].

4. Results

4.1. Geotechnical Data

The analyzed Georgian monastery complexes are carved in soft rocks such as tuffs (Vanis Kvabebi) and sedimentary transitional-marine formations (David Gareja and Uplithsikhe). From a geotechnical point of view all the collected samples are characterized by very low strength parameters (many samples were easily broken even by hand), particularly for the David Gareja samples, showing that these rocks are very weakly cemented (Table 3). The geotechnical characterization of volcaniclastic tuff material at the in-situ scale is affected by several issues, such as the large dimensions of the clasts, reduced strength contrast between the matrix and the clasts themselves [80,81]. Regarding the Monastery of Petra thin sections of Upper Umm Ishrin sandstone shows multicolored, fine to medium, subangular to sub-rounded grained sandstone [82]. Mineralogical-geotechnical data from [44] report iron oxides and kaolinite are the main rock matrix, while quartz grains make up over 80% of the stone content. Porosity is moderate, with total porosity around 15% and mainly medium (1–10 μm) to coarse pores (10–100 μm). According to [16] the UCS values of the monastery are around 25 MPa, showing that all the analyzed rupestrian sites are also constituted by weak rocks.

Table 3. Average values of the obtained geotechnical parameters of the collected samples.

| Case Study	Friction Angle (°)	Uniaxial Compressive Strength (MPa)	Unit Weight (KN/m^3)
Vanis Kvabebi	28°	2.70	16.76
Natlismcemeli	27°	0.49	16.56
Sabereebi	23°	0.52	15.09
Uplistsikhe	40	3.55	19.5

4.2. Field-Remote Surveys and Kinematic Analysis

4.2.1. Vanis Kvabebi

Besides the sub-horizontal layer bedding, three main subvertical joint sets were identified (Figure 6a): (1) J1: dipping W and N-S oriented, forming the main slope faces (Figure 6d); (2) J2: dipping NW and SW-NE oriented, it is responsible for the formation of a master joint intersecting all the upper section on the eastern rock wall of the complex; (3) J3: dipping SE and trending NW-SE, it represents persistent fractures along which ephemeral creek erosion has caused deep channel cuts in the southern sector of the complex (Figure 6e).

The field surveys highlighted differential erosion as an important local predisposing factor of instabilities, creating large niches along the bedding, especially in correspondence of the softer and more erodible ash layer and the upper section of the medium-grained tuffs, therefore undermining the overlying overhanging cliff sectors. In this framework the main identified high angle joint sets (Figure 6a), combined with the stratigraphic features worsened the cliff instability: J1, dipping W parallel to the cliff face determines planar failures (Figure 6b,d) especially affecting the overhanging sectors within the tuff layers, while the combination of J2 (dipping NE) and J3 (dipping SW) cause wedge failures (Figure 6c), occurring especially in correspondence of the more competent welded tuff sectors (Figure 6f). The 2D-orthoprojection and the performed hydromodelling allowed the investigation of the complex drainage pattern of the ravine, with streams categorized

by catchment area and order (Figure 7a). Very low order rivulets develop on the main cliff (eastern sector) along the J3 fractures (Figure 7a–c), as well as the main streams located in the southern sectors, which deeply cut into the volcanic sequence along large erosion channels involving the whole cliff height (Figures 6e and 7a). In particular, stream erosion acts along the J3 master joint creating potentially unstable niches at the base of the medium-grained tuffs (Figure 7d).
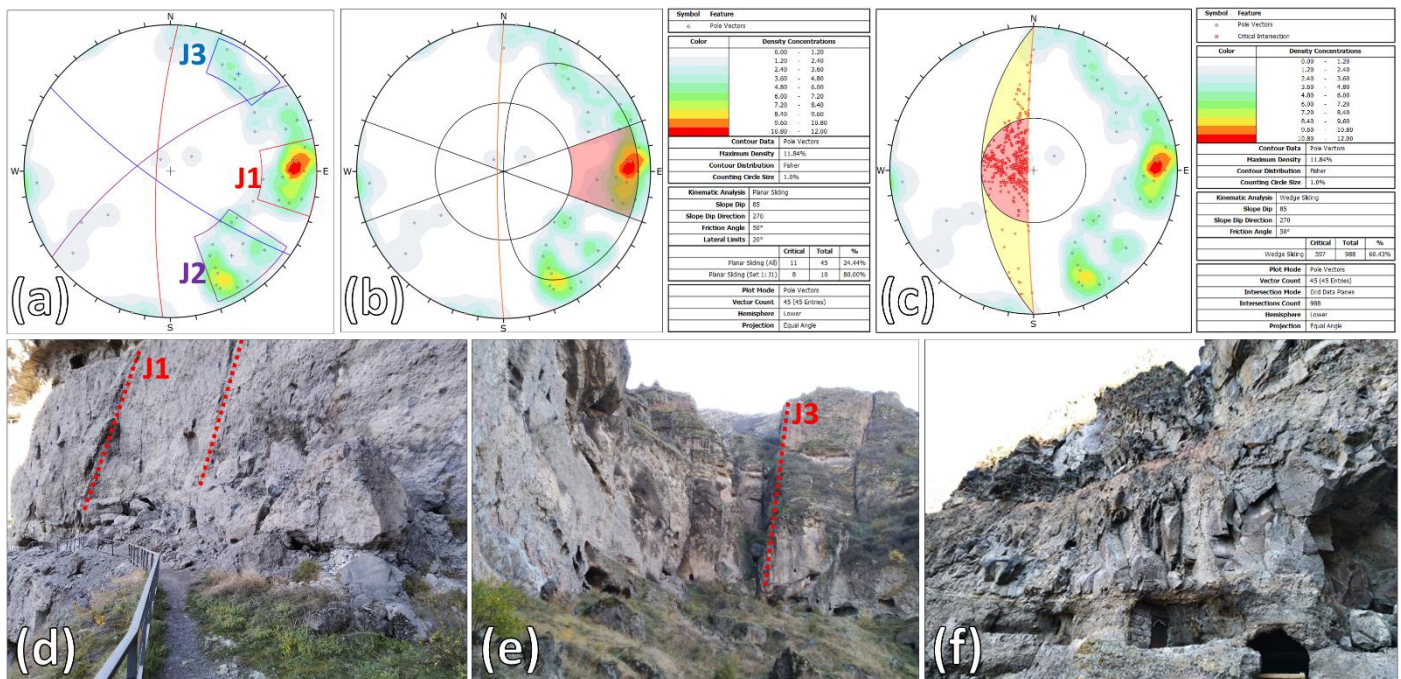

Figure 6. Structural setting and kinematic analysis at Vanis Kvabebi: identified sets (**a**); kinematic analysis for planar (**b**) and wedge (**c**) failures; 2017 rock fall deposits (**d**); subvertical fracture where creek channel erosion has concentrated (**e**); welded tuff portion affected by wedge failures (**f**).

The IRT surveys were carried out from a 100 m distance, leading to a 1120 × 1460-pixel image with 6.5 cm pixel size. Several thermograms were mosaicked creating a surface temperature map of the main part of the eastern cliff face (Figure 8a). A temperature gradient is visible from top to bottom (Figure 8b): the upper basalt flow portions show higher temperatures (3.4 °C), due to a more direct sunlight radiation with respect to the lower medium-grained tuff level (2.4 °C), and especially the coarse-grained tuffs, more shaded and cooler (1.9 °C), also due to the presence of grass cover at bottom of the ravine. Warm anomalies were highlighted in correspondence to the ledge-niche systems in the upper basalts and the cave system (4.4–6.5 °C), the eroded lower part of the basalt flows (4.2–5.6 °C), and along which the second level pathway develops but especially where the master joint belonging to J2 intersects the whole lower basalt portion. Regarding this open fracture (over 40 m persistent) the IRT data allowed for the description of the aperture geomechanical parameter as from extremely wide (10–100 cm) to cavernous (>100 cm) according to [12]. In correspondence to the 2017 rock fall niche (AOI 1 in Figure 8c), no evidence of moisture/seepage phenomena was detected; therefore, dry conditions were assessed during the survey (Figure 8a,c).
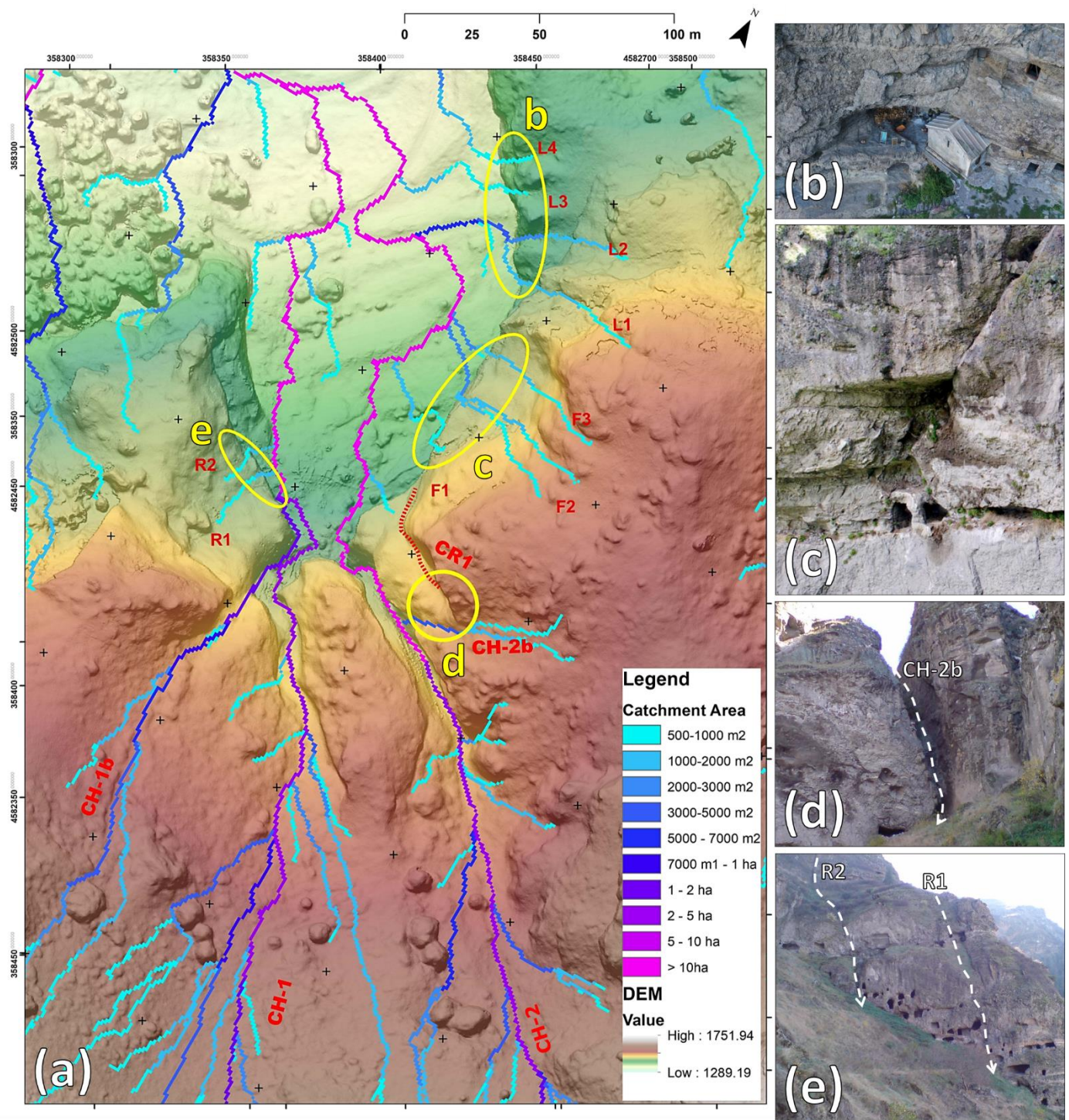
Figure 7. Vanis Kvabebi surface water run off model: (**a**) 14 cm resolution DSM with streams categorized by catchment area (ovals highlight details in b-e; stream legend: L = left cliff; F = front cliff; R = right cliff; CH = channels); (**b**) top-view of the lower chapel area; (**c**) Large niche created by erosional features of the J2 set Master Joint; (**d**) erosional channel in correspondence of J3 fracture; (**e**) stream gullies on the slope of the ravine opposite the monastery.
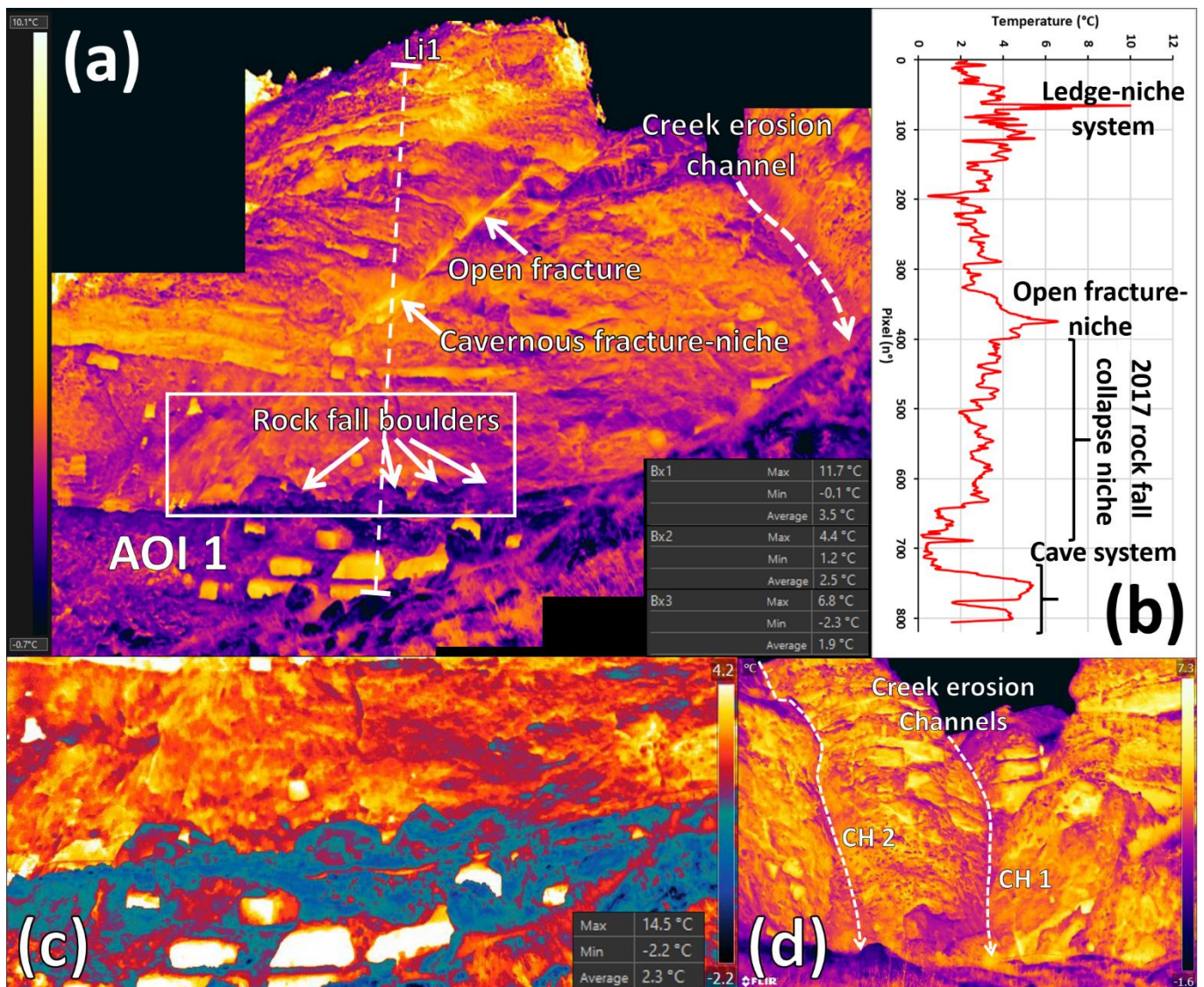
Figure 8. Vanis Kvabebi IRT data: mosaicked surface temperature map of the main sector of the eastern cliff (**a**) (the white rectangle represents the Area of Interest 1 = AOI 1 shown in (**c**)); vertical surface temperature profile of the cliff (**b**) (Li1 in **a**); detail of the 2017 collapse sector (AOI 1) (**c**); surface temperature map of the cliff's southern sector (**d**).

Cold thermal anomalies were detected along creek erosion channels (Figure 8a), especially in the cliff's southern sector (Figure 8d), due to the presence of moisture connected to ephemeral rivulets. The 3D kinematic analysis performed shown in Figure 9 covers the area represented by the 3D model of Figure 2b. The color scale represents the 3D spatial probability of occurrence (expressed in %) for the different instability mechanisms, with colors ranging from blue (very low probability) to red (high probability), for the most relevant detected instability mechanisms affecting the rock cliff, which are: wedge failure (Figure 9a), followed by plane failure (Figure 9b), and subordinately free fall (Figure 9c).
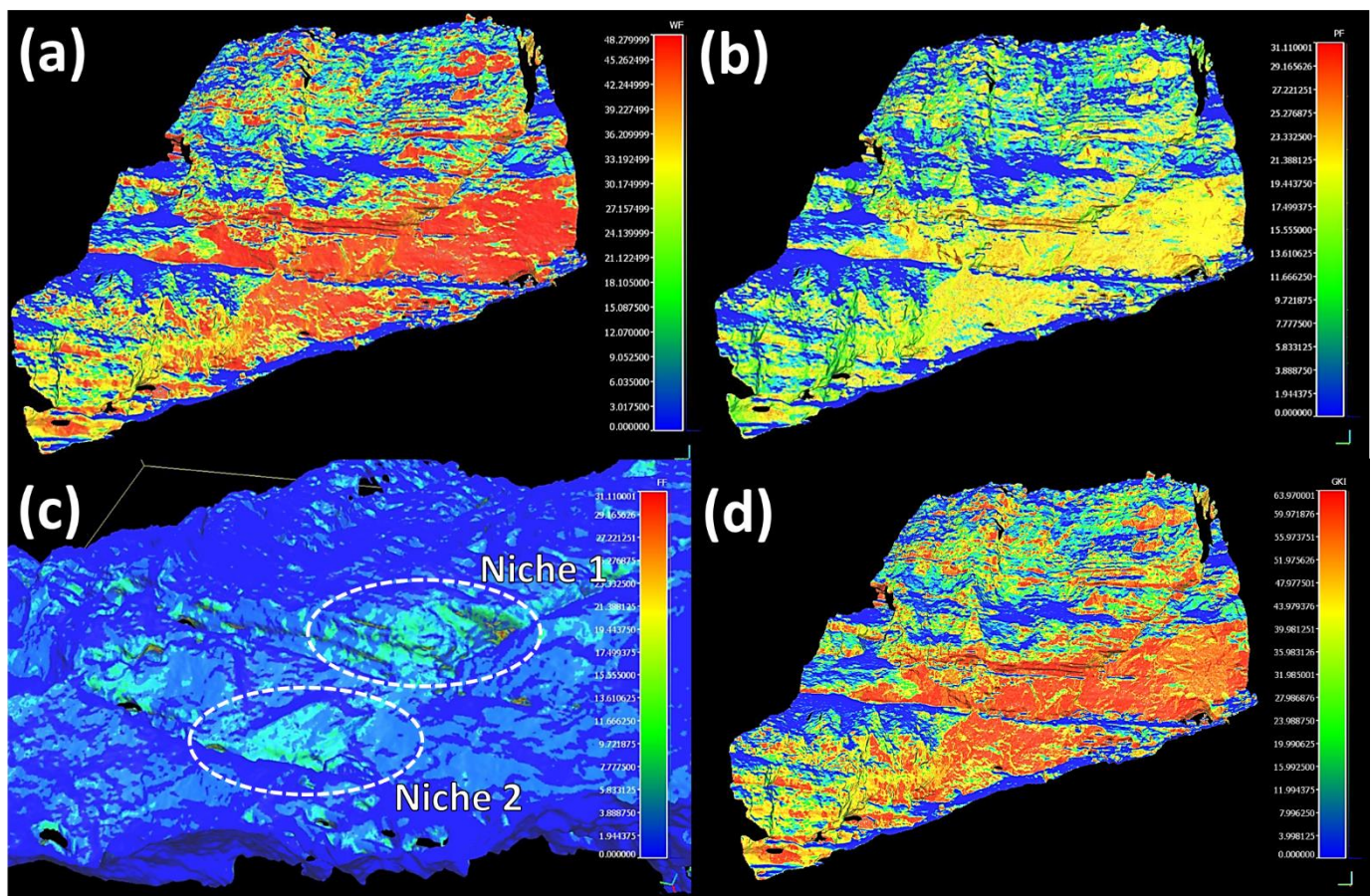
Figure 9. Results of the 3D kinematic analysis. Wedge failure = 48% (**a**); planar failure = 31% (**b**); free fall = 31% (white ovals highlighting the detected unstable niches) (**c**); GKI up to 62% (**d**).

The latter can be locally predominant in overhanging sectors, such as the large niche created by erosional features of the J2 set master joint in Figure 7c (Niche 1 in Figure 9c), and the 2017 collapse niche (=AOI 1 in Figure 8a,c; Niche 2 in Figure 9c,). In general, the cliff is highly prone to kinematic instability mechanisms (GKI max > 60%, Figure 9d), especially along the lowermost basalt flow portion and the ash layer within the tuff, along the niches and the master joint.

4.2.2. David Gareja

Hereafter the outcomes of the surveys on the sites of Natlismcemeni and Sabereebi are presented. Like many of the monasteries of David Gareja, the Natlismcemeni complex (still inhabited by a monastic community) is located on top of a hogback ridge overlooking a low hilly landscape and is mainly carved in a 40 m high rock cliff. The latter is formed by a 20 m-thick sequence of thin alternating layers of fine-grained sands and clays capping a 20 m-thick level of coarse-sand layers; a debris talus discontinuously mantled by sparse bushy vegetation covers the lowermost part of the sequence (Figure 10a). The monastery's main spaces (chapels and monks' cells) are represented by three levels of over 30 caves cut into the thick weak sandy layer, while additional brick construction works are placed either on top of the sequence (tower) or adjacent to the cliff face (a new chapel and storage rooms; Figure 10a). The main discontinuities are organized in two main joint sets: J1 is related to the bedding and dips NE against the slope with low angles; J2 is a mainly subvertical set dipping SW along the slope; J3 is a subvertical fracture sparsely cutting the cliff face (Figure 10b). These fractures have a fundamental control on the stability of the cliff, as testified by detached large blocks deposited at the foot of the cliff on the northern sector of the cliff face (Figure 10a). The performed 2D kinematic analysis allowed for assessing the

main instability mechanisms affecting the rock cliff, which are represented by plane failure, followed by wedge failure and subordinately by toppling (Figure 10c–g).
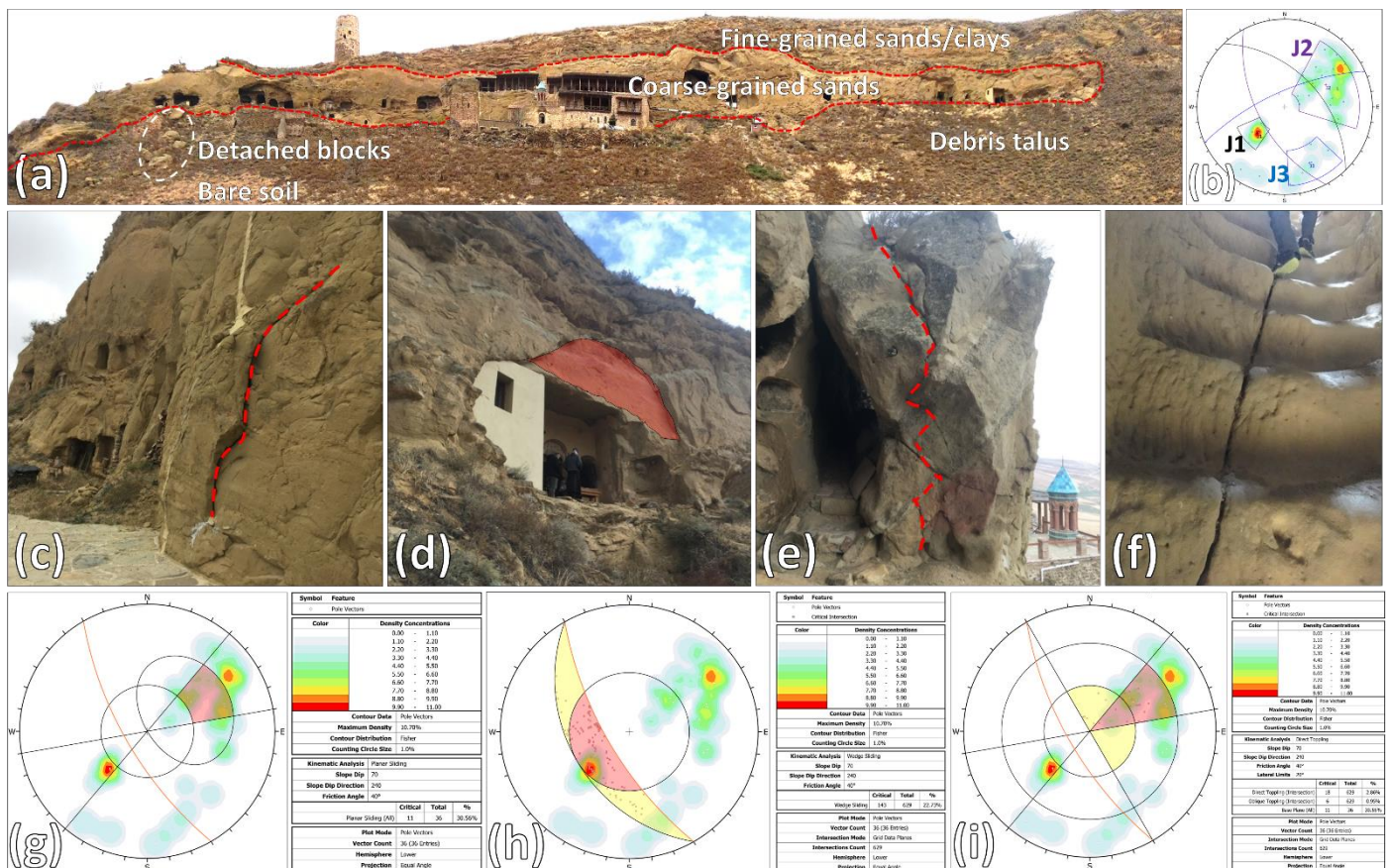

Figure 10. Outcomes of the field surveys in the Natlismcemeni monastery: local geological features (**a**) and structural discontinuities (**b**). Main instability phenomena detected in the field surveys and corresponding 2D kinematic analysis: planar (**c**,**g**) and wedge (**d**,**h**) failures; topples (**e**,**i**). Open fracture (**f**).

Wedge failures can be locally predominant in overhanging sectors, such as the cave niches (Figure 10d–h), while open fractures parallel to the slope can develop topples (Figure 10e,i). Very persistent and spaced wide-open fractures are visible within the monastery caves and can potentially damage the complex seriously (Figure 10f). The IRT survey was carried out from different acquiring positions (at a 110 m and 20 m respectively; Table 2) in order to cover the whole complex (Figure 11a) and make close-ups on critical sectors (AOI2, 3 in Figure 11b,c).While the sound rock slope shows average values between 10.2–10.8 °C, warm thermal anomalies (13.8–14.1 °C) were widely detectable both at the top of the thick sandy layer related to J1, and at the topmost sector of the cave accesses, highlighting potentially unstable ledge-niche systems (Figure 11a–c). Warm thermal anomalies also enhance wide open fractures located parallel to the slope (related to J2; Figure 11b,c). No cold thermal anomalies were detected; therefore, dry conditions were assessed at the time of the survey for the site. The 3D kinematic analysis confirms how the more unstable slope sectors are located in correspondence to the ledge-niche systems, where GKI reaches up to 64% (Figure 11d).

The monastery of Sabereebi (currently abandoned) is composed of a series of 15 frescoed caves (Figure 12a) developed on three levels carved in sandy layers. As for Natlismcemeni, Sabereebi is located on top of a hogback ridge carved in material formed by a transition between very weak sandstones and partially cemented sediments, represented by a sequence of conglomerates at the top, a 10 m-thick level of coarse-grained sands overlying a sequence of alternating fine-grained sands and clays; a sparsely vegetated

debris talus covers the slope toe (Figure 12a,b). In fact, some sandy blocks were found at the foot of the talus during the 2018 field survey, one of them evidently freshly detached from a pillar formed by the intersection of J2-J3 (Figure 12a,c,d). The bedding (J1) dips NE towards the slope with low angles, while two not widely spaced but persistent discontinuity sets cut the slope parallel (J2) and orthogonal (J3) to the cliff face, dipping E and SSW respectively, deeply affecting the stability of the cliff (Figure 12e). The 2D kinematic analysis confirms high planar and especially wedge failure indexes along these planes, subordinately toppling (Figure 12c–f).
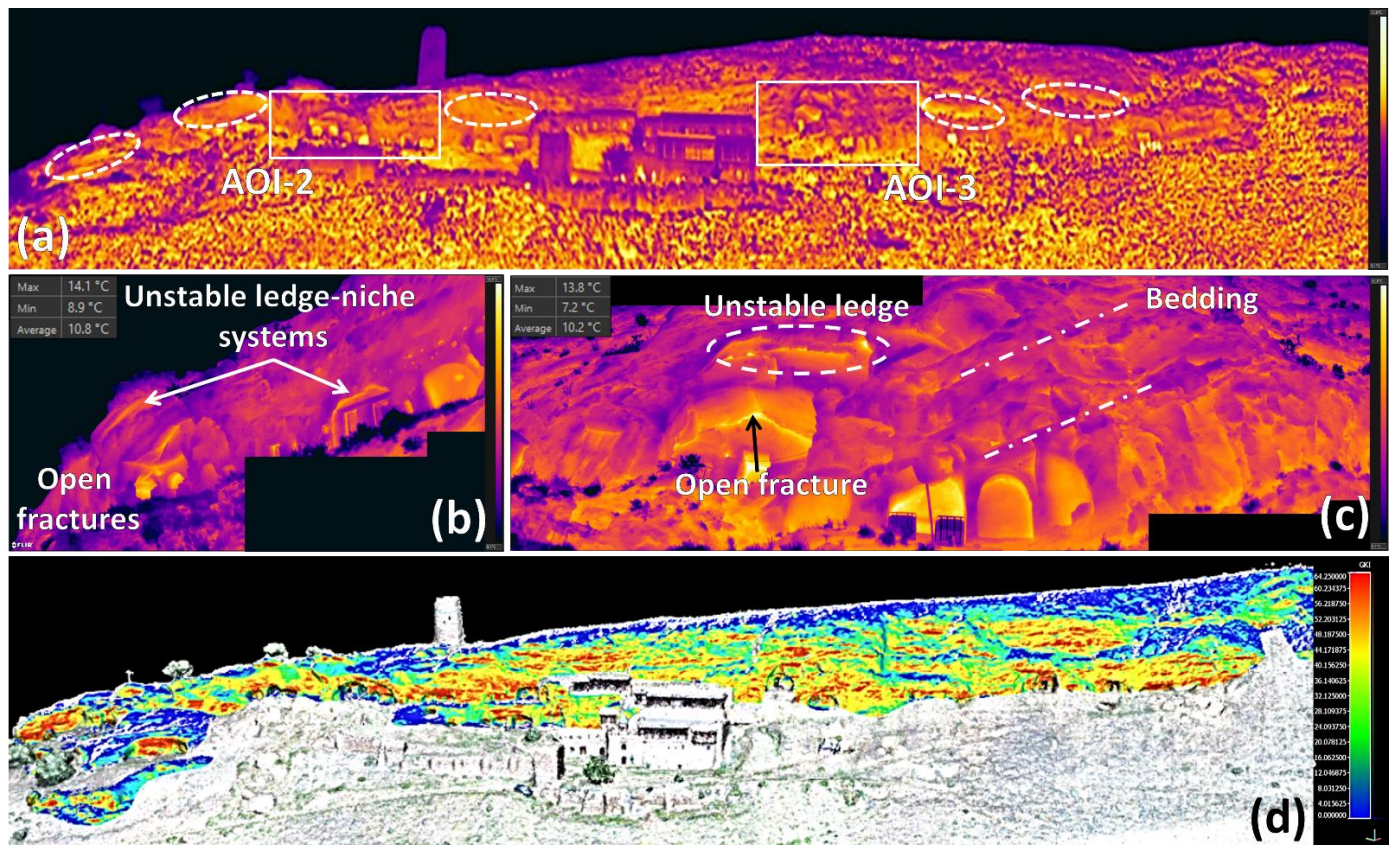
Figure 11. Outcomes of the IRT surveys of the Natlismcemeni monastery: IRT mosaicked image (2075 × 505 pixels with 7.1 cm pixel size) showing the detected AOI 2–3 (white rectangles) and the warm thermal anomalies (dashed white ovals) (**a**); AOI 2 (1160 × 480-pixel image size) (**b**) and AOI 3 (2120 × 590-pixel image size) (**c**), both having 1.3 cm spatial resolution; 3D kinematic analysis (GKI index up to 64%) (**d**).

IRT surveys were carried out from 100 m and 20 m (Table 2) to map all the monastery cliffs and make detailed analysis on AOIs. IRT analysis showed average temperatures of 26.8 °C of the slope face and warm thermal anomalies (from 31 to 42 °C) in correspondence to the recent collapse sector and the underlying slope talus (AOI 4), where erosion is exposing bare soil (Figure 13a,b,d). Sharp cold thermal anomalies (15.4–17.7 °C) highlight a large system of open cracks connected to J3 at the right end of the complex (AOI 5; Figure 13a,c,e). As for Natlismcemeni, no cold thermal anomalies were detected; therefore, dry conditions were assessed at the time of the survey.
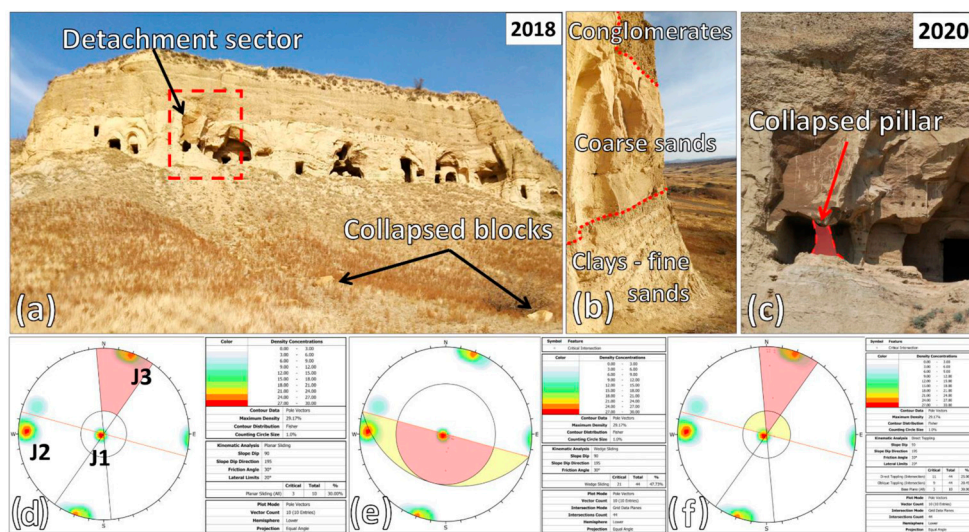
Figure 12. The Sabereebi monastery geological features: cliff face showing the chambers and the detached block in 2018 (**a**); stratigraphic sequence (**b**); the detachment sector in 2020, showing the collapsed pillar (**c**); 2D kinematic analysis: wedge failure mechanism (**d**); planar failure mechanism (**e**); direct toppling (**f**).
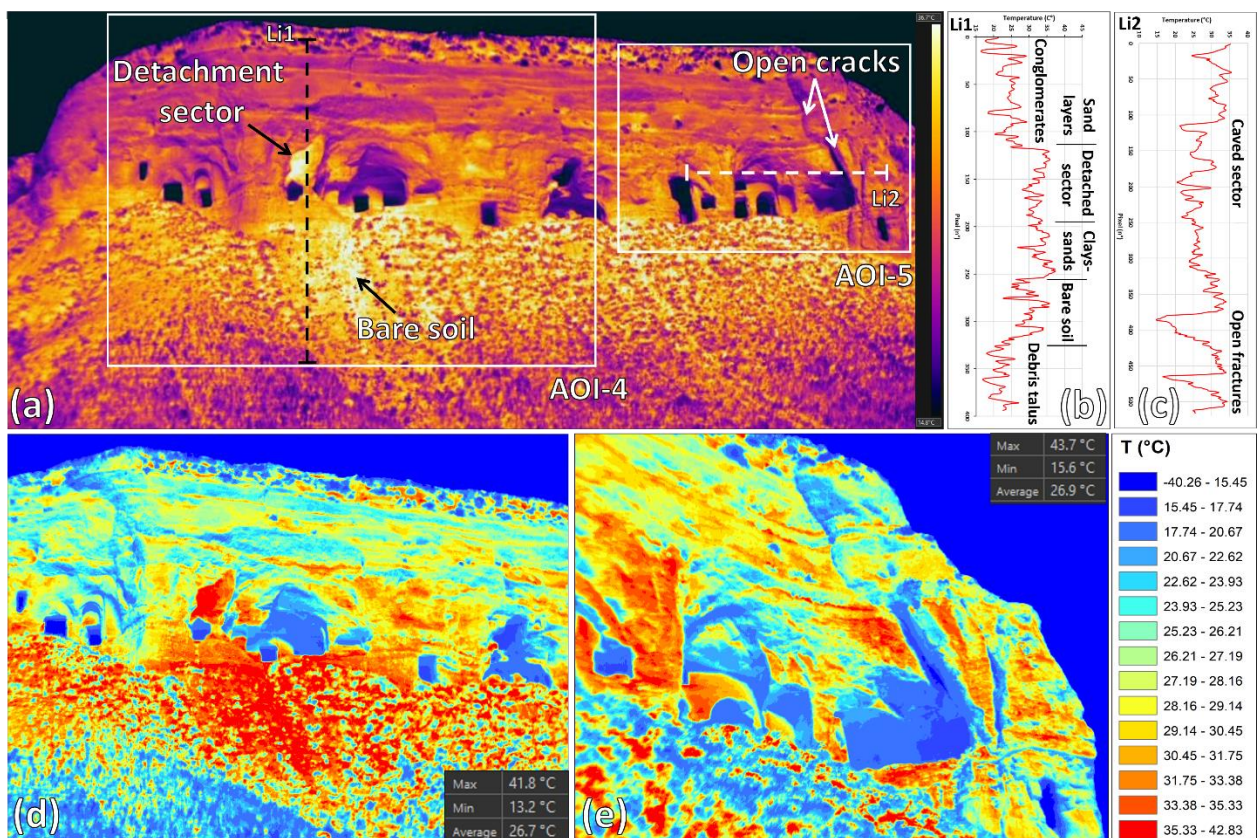
Figure 13. Sabereebi IRT data: Mosaicked surface temperature map (950 × 480 pixels with 6.5 cm resolution (**a**); vertical and horizontal surface temperature profiles Li1 (**b**) and Li2 (**c**). Classified surface temperature maps in correspondence of AOI 4 (**d**) and AOI 5 (**e**).

The UAV-DP survey and the hydromodelling analysis provided a high-resolution DEM and derived products such as slope and the drainage maps (Figure 14a,c). These latter showed main cataclinal-type streams draining the hogback of the monoclinal structure to the NE, while small anaclinal-type streams erode the debris talus underlying the monastery,

as shown by the bare soil sectors highlighted by IRT. Therefore, linear erosion does not affect the cliff face of Sareebebi, although field surveys highlighted traces of mud drips on the cliff face coming from the top of the hogback, showing that overland flow can affect the monastery during rainfall events (Figure 14b).
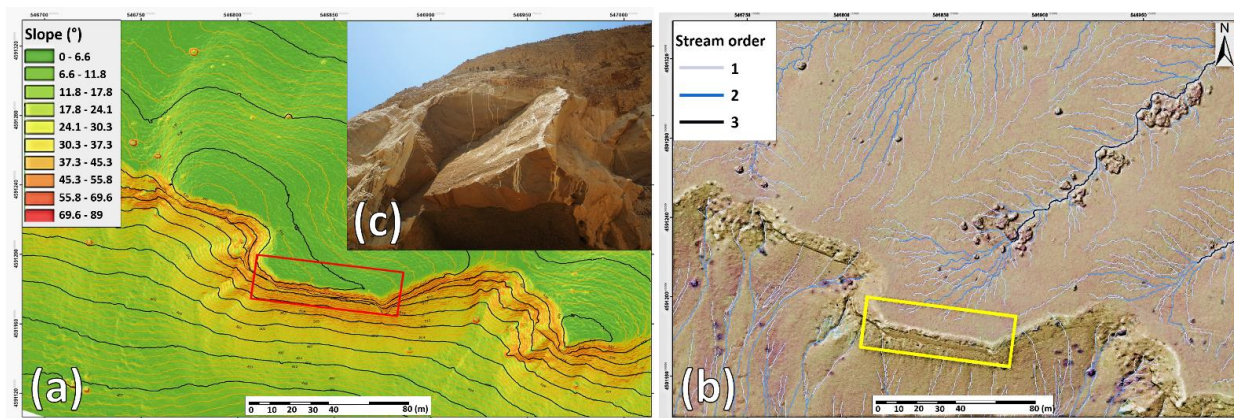

Figure 14. UAV-DP high resolution DEM derived products: slope map (**a**) (the monastery complex is located by the red rectangle); drainage pattern map (**b**) (the monastery complex is located by the yellow rectangle); UAV close-up on the detachment sector showing light brown colored mud drips on the dark brown sandstones (**c**).

4.2.3. Uplistsikhe

Four main identified discontinuity sets were identified in the field: J1 (bedding) dips SE with low angles, J2 joint set dips SW parallel to the slope face with high angles, J3 is a subvertical joint set trending WNW-SSE and J4 dips NW with mid-high angles (Figure 15a). The 2D kinematic analysis highlighted two equally predominant instability mechanisms: plane (Figure 15b) and wedge failures (Figure 15c). In general, the rock cliff is highly prone to kinematic instability mechanisms (GKI max = 50%, Figure 15d), particularly the areas affected by the June 2018 and the November 2019 failures (Figures 4c and 15d).
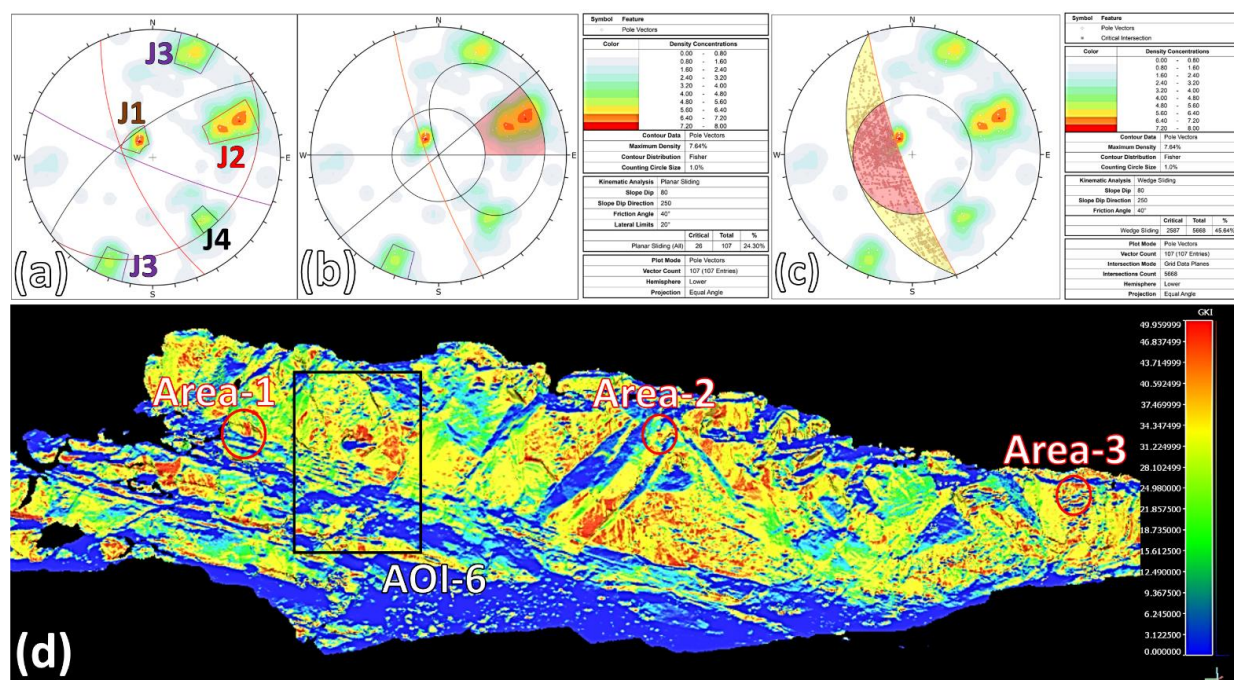
Figure 15. Structural data in the site of Uplistsikhe: main discontinuity sets (**a**); 2D kynematic analysis for planar (**b**) and wedge failures (**c**); 3D kynematic analysis (GKI index up to 49.9%) (**d**), showing the areas affected by rockfalls (Areas 1–2 in the red ovals), and the AOI highlighted in Figure 16 (black square).
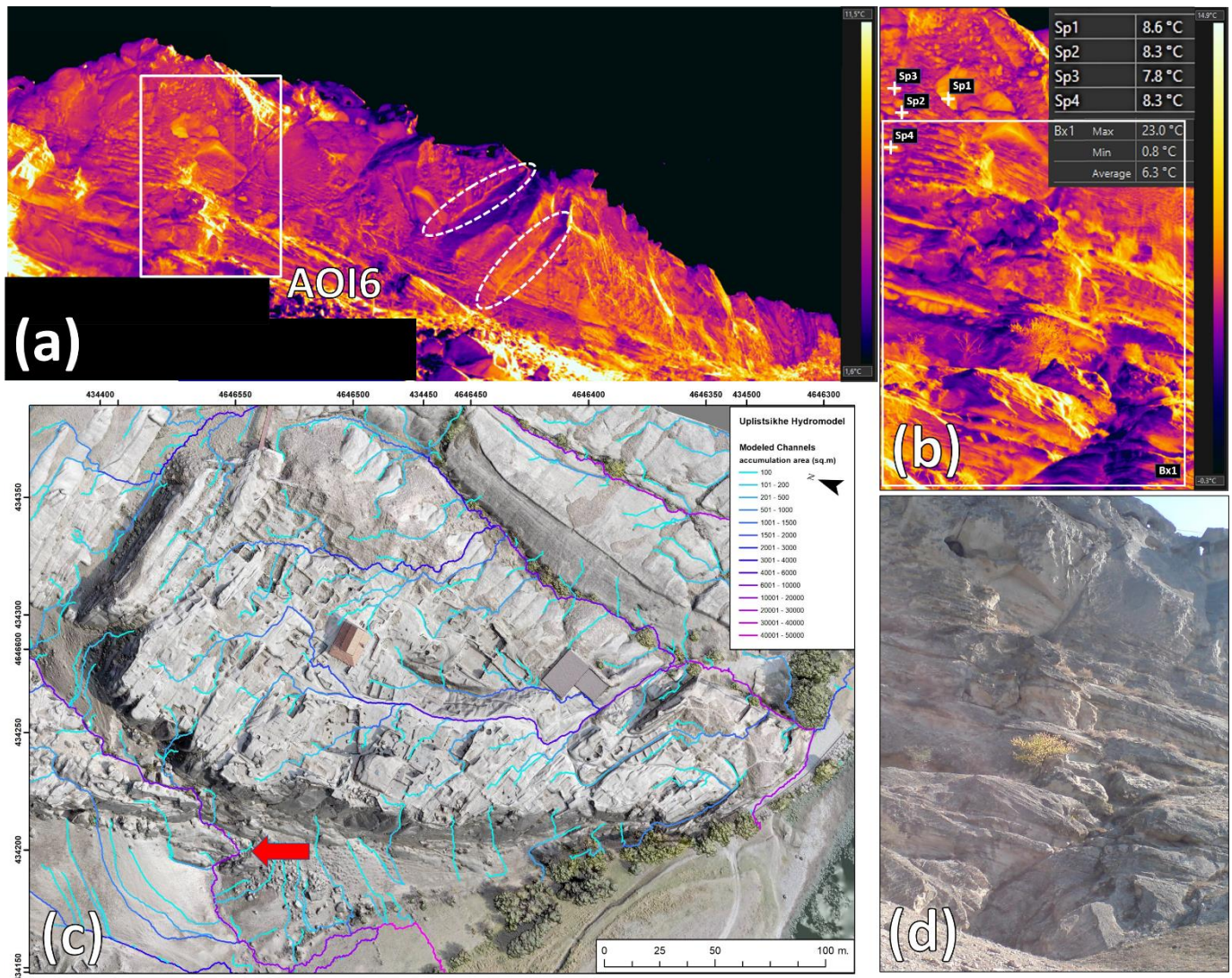
Figure 16. Outcomes of the IRT surveys: mosaicked thermograms (2800 × 850 pixel) (**a**) showing open fractures along J4 (white dashed ovals) and AOI 6 highlighted in b, d; detail of the cold thermal anomaly (**b**) with spots showing the warm thermal anomalies where the corrasion cavities develop (Bx = box plot showing min., max., avg. temperature); modelled ephemeral drainage network of the site (**c**) (red arrow highlights the ephemeral stream developing the cold thermal anomaly in **b**); correspondent optical image of b (**d**).

The IRT survey highlighted warm thermal anomalies along persistent joints belonging to J4, where minor rock falls occurred in 2019 (Figure 16a). General dry conditions were assessed along the rock cliff except for the left sector, where a cold thermal anomaly (as well as the presence of vegetation and weathering coating) revealed the presence of an ephemeral stream, which concentrates along J4, the rock cliff's most persistent discontinuity set (AOI 6 in Figure 16b,d). This is confirmed also by the hydromodelling analysis (red arrow in Figure 16c), which also shows how the high order ephemeral streams concentrate mainly along J3-J2 sets, while low order ephemeral streams mainly along J4. The exception is represented by the detected cold thermal anomaly located in correspondence to a high order main stream developed in a very persistent and eroded discontinuity belonging to J4. AOI 6 is also characterized by warm thermal anomalies enhancing cavities of various size caused by corrasion (Figure 4d, spots = Sp1–4 in Figure 16b) and is particularly prone to instability, as shown by the high GKI values (Figure 15d).

4.2.4. The Monastery in Petra

The IRT surveys allowed the mapping of evident widespread cold thermal anomalies along an alignment which extends continuously from the left-bottom sector of the of the rock wall to the left basal part of the monastery (Figure 17a). Seepage is particularly evident in the left sector of the rock wall with respect to the adjacent lower left part of the monument, as shown also by the vertical surface temperature profiles (Figure 17b,c,e–g). The analysis of the average temperature confirms this trend: while on the dry rock wall temperatures range from 20.1 to 20.3 °C (Bx 1 in Figure 17d,h), in the damp area varies from 19 to 19.4 °C (Bx 2 in Figure 17d,h), while there is a marked drop in correspondence to the seepage sectors (from 13.4 °C to 15.5 °C), especially in the rock mass at the left of the monastery (see Bx 3 in Figure 17d,h).
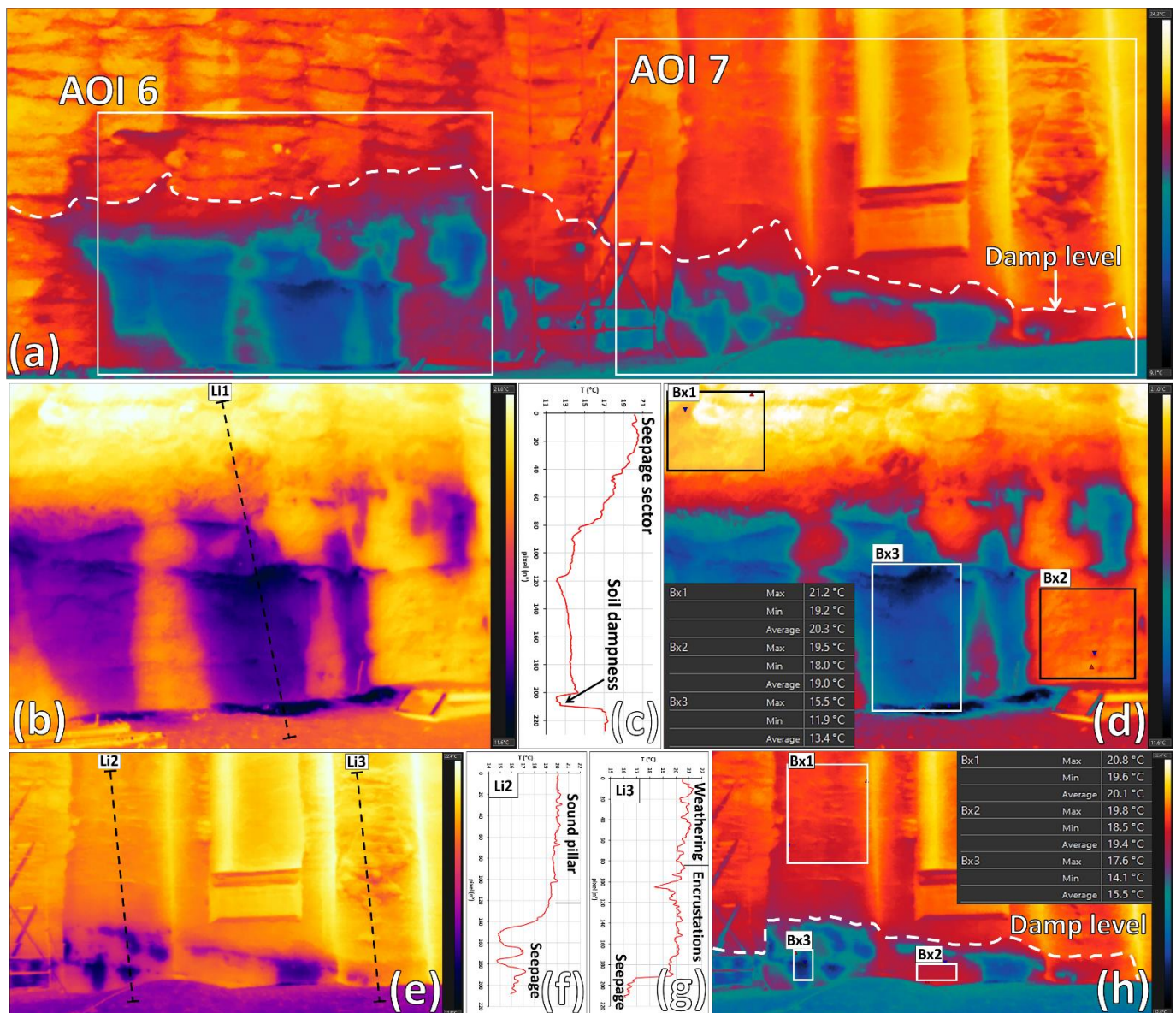
Figure 17. Petra Monastery IRT data: mosaicked thermal image of the low-left corner of the monastery (680 × 240 pixels; corresponding optical image in Figure 5c) (**a**); close-up single thermograms (320 × 240 pixels): AOI 5 (**b–d**) and AOI 6 (**e–h**).

5. Discussion

5.1. Conservation Problems Affecting the Analysed Rupestrian Sites

Authors like [13,16] report the relationships between UCS and porosity in the rocks of some important rupestrian sites part of the UNESCO world heritage or tentative lists, including Vardzia in Georgia (geologically very similar with respect to Vanis Kvabebi) and Petra. They demonstrate how the low UCS values are generally coupled with high porosity, especially in volcanic materials, for example the ones of Vardzia, which are part of the same geological formation of Vanis Kvabebi. On the other hand, the continental/sedimentary geological formations, such as the soft sandstones of Bamiyan (very similar to the ones of David Gareja) and Petra, exhibit a relevant vertical heterogeneity due to the formation's stratigraphy. From a geotechnical point of view the arrangement between the tuff components, their different fabric, and the normally large amounts of clay minerals in the matrix opens a very wide spectrum of porosities. This can play a key role in the behavior of the rock resistance to weathering and deterioration due to moisture [6,7]. Moisture expansion under determinate relative humidity (hygric dilatation) is caused by the swelling and shrinking of clay minerals (originating from the chemical decomposition of silicate minerals of the weak rocks) and can be recognized as one of the most important factors contributing both to the weathering and deterioration of both volcanic tuffs and sandstones [5,8,9,83]. In particular [8] demonstrated how the intensity of moisture expansion and related swelling pressure cannot be attributed only to the swelling of clay minerals, suggesting that the micropores and the resulting disjoining pressure during wet/dry cycles also play an important role. Moisture expansion also leads to the reduction of the uniaxial compressive strength of the tuff when saturated [10,11]. Therefore, water runoff, concentration, and seepage can trigger these degradation phenomena within weak and porous material such as the tuffs and sandstones of the analyzed sites. Furthermore, in rupestrian sites areas of preferential water runoff are governed by the slope morpho-structural setting, being caused by the combination of the fracture system (especially the open features), and the slope-scale morphology-roughness (e.g., ledges and niches and unstable protruding-overhanging sectors) [13]. Joints and cracks in particular can also affect the structural stability of tuff slopes, since their geometry with respect to the slope face generates different kinematic behavior of the rock mass, while their engineering properties are adversely affected by water seepage and moisture, causing weathering and discoloration films reducing the wall strength [9,10,17]. This process can lead to the loosening of the rock mass and the widening of the joints creating potential instabilities such as open features [12]. Water is also a major factor in the deterioration process in Petra, due to flood damage, rainwater, runoff water, capillary action, and their subsequent effects such salt encrustation on the sandstone surface [40,82,84]. The rising of the water table in the area in particular has had a major impact on many other deterioration mechanisms such as salt crystallization due to water evaporation and the dissolution or leaching of materials (clay minerals, for example, since most of the Petra monuments were carved from sandstone with a high clay content) [85]. Salt-crystal encrustation can also expand and widen existing fissures, triggering rock-falls and collapses; this process is known as salt-wedging and is a great contributor to the degradation of Petra's archaeology and natural features [86,87].

5.2. Conservation Criticalities and Proposed Mitigation Measures

5.2.1. Vanis Kvabebi

The performed analysis confirmed that the 2017 rock fall event occurred in presence of a strong structural control due to the collapse of a protruding sector of the basal sector of the medium-grained tuffs; this was undermined by an erosional niche in the underlying ash layer, J1 joints, and a master joint belonging to J2, characterized by high persistence involving the whole upper cliff sector (from the medium-grained tuffs to the basalt flows; Figures 6–9). The modelled stream pattern is connected to rainfall and is governed by the interaction of water runoff with the morpho-structural setting of the slope, allowing analysis of damage pattern and detection of substantial water driven erosion. The J2 master-

joint is a key fracture for the stability of the cliff, since the hydromodelling shows how it acts as a concentration area for water runoff, which in turn causes linear stream erosion that keeps widening the joint. This process has gone to the point of creating a concentration of water runoff which in turn has generated an unstable niche in the lower portion at the contact with tuffs, where basalts are more erodible (Figures 7c and 9c). Vanis Kvabebi in general shows distinct marks of rainwater weathering and erosion processes: nearly all recent collapses are connected to heavy rainstorms, as reported by local monks. Water stream gullies observed in situ completely match with the stream trajectories outlined in the hydromodelling, confirming water runoff/concentration as the most damaging factor in the site. Based on these outcomes a water drainage system was designed using the obtained high-resolution 3D model as a topographic reference base, in order to design appropriate plans and cross-sections.

The modelled streams were classified in a GIS environment [63] according to the number of confluences and the watershed areas. The main streams are represented by two main channels (Ch1–2 in Figure 7a, of which watershed areas are 5.5 and 6.5 Ha, Figure 18a). Both channels are fed from the steep slopes (approximately 200 m vertically) on top of the Vanis Kvabebi volcanic tuff-breccias in which they cut deep gullies (Figure 8) and are not much affected by runoff coming from the Javakheti Plateau (only 1 Ha of the 6.5 Ha watershed comes from the Javakheti Plateau; Figure 18a). Due to the depth of the gullies, it is practically impossible to divert water from them. Smaller streams (L1–4 and F2-3 in Figure 7a) develop on the monastery's main eastern cliff, their watershed surface varying from 330 to 2670 m^2 (Figure 18a). The action of these streams, with special regards to the ones with watershed areas 770, 550, and 2230 m^2 have a great impact on the weathering, erosional features, and stability of the monastery. As shown by the analysis of the DEM, despite the complex nature of the relief, most of the observed water streams can be diverted from the main cliff by directing them to other parts of the rock cliff (Figure 18b). Based on the existing DEM the alteration of hydrographical model for the proposed water diverting wall was calculated.
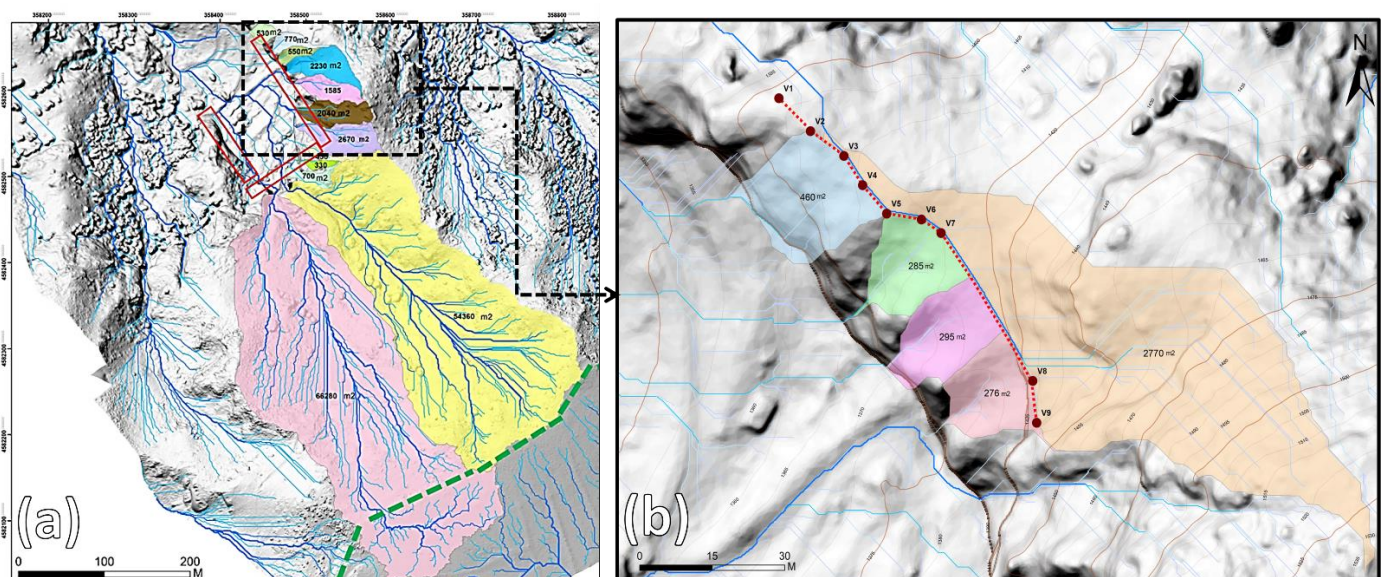

Figure 18. Vanis Kvabebi mitigation measures: hydrographic model (**a**) showing the watershed surfaces, the rock cliff areas (red rectangles), the area where the water drainage system (shown in **b**) is planned (dashed black square), and the Javakheti Plateau divide (dashed green line), (map of the planned water diverting wall (dashed red line) (**b**).

The results show that the proposed wall will ensure the water diverting of an area of 2770 m^2 area, while the minor stream catchment areas will be reduced to values ranging from 276 to 460 m^2 (Figure 18b). The water diverting wall (about 90 m in length) will be constructed using local material to minimize its visual impact. The area is easily accessible

by a pedestrian path from the opposing side of the cliff, while only the first 15 m section will require scaffoldings, being placed on a rock cliff. Thus, mitigating rainwater impact will considerably reduce active hazards on the given area.

5.2.2. David Gareja (Natlismcemeni and Sabereebi)

Generally, there is not a predominant instability process acting in the analyzed sites: they can all be attributed to rock collapses directly dependent on the local structural setting differently interacting with the slope face and stress release. In Natlismcemeni the performed activities proved to be effective tools for the location of potentially unstable ledge-niche systems and open fractures and to define the more landslide-prone sectors as priority areas for sealing/reinforcement. In Sabereebi erosional processes caused by ephemeral streams in the debris talus can undermine the stability of monastery pillars (as shown by the recent collapse; Figures 12–14). Future mitigation works to be planned are drainage channels to avoid both overland flow on top of the rock slope and stream erosion of the underlying debris talus. Rock samples collection and laboratory tests are still ongoing, and they will define the main strength and deformation parameters useful for future stability models. Nonstructural mitigation actions, such as the implementation of a monitoring system to measure the displacements, such as robotized topographic stations and Ground-based Synthetic Aperture Radar systems are being implemented (Figure 19a,b). Such action is important for establishing the priorities in the areas of intervention, in the framework of the site's preservation, as well as for the safety of local monks, for the staff of rock-climbers which will be operating in reinforcement/conservational tasks in the near future and for visiting tourists.
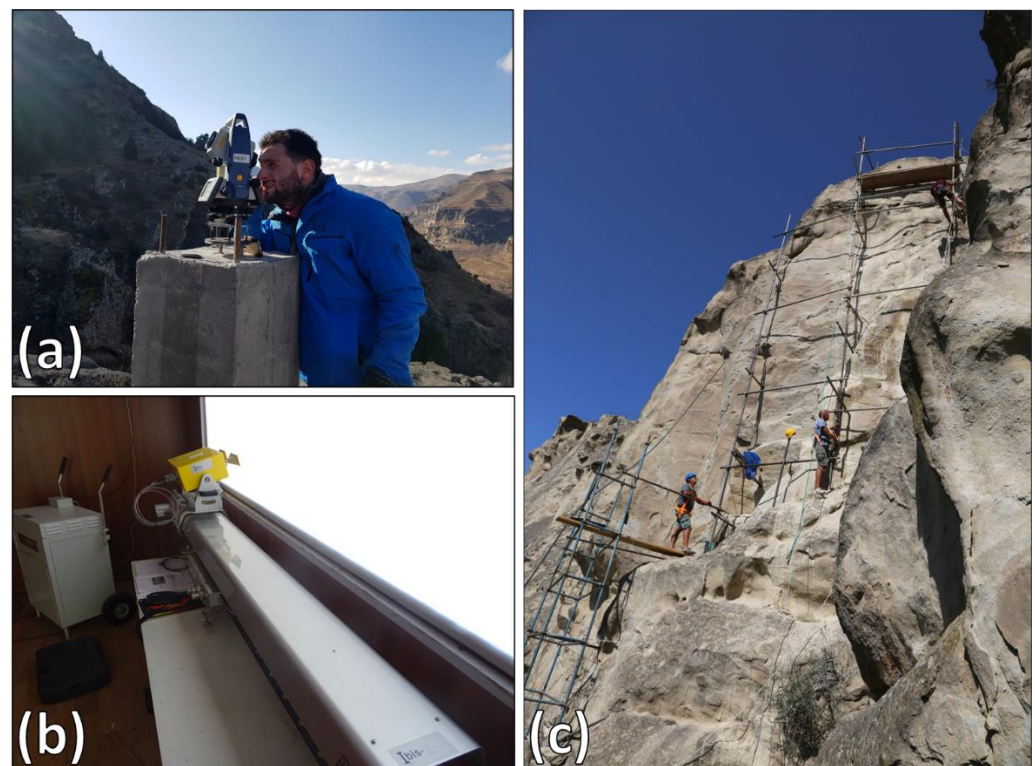
Figure 19. Nonstructural measures, such as displacement monitoring systems, planned in David Gareja: Robotized Total Station (**a**); ground based interferometric synthetic aperture radar system (**b**). The scaffolding constructed for the anchoring phase in Uplistsikhe (**c**).

5.2.3. Uplistsikhe

Several critical areas (Figures 15 and 16) among which the rockfall-affected areas (Areas 1–3 in Figure 15d) were selected as the highest priority for the consolidation works

and for monitoring. These started from Area 1 with the reinforcement of a critical block on the rock cliff, by means of deep anchoring. A special hanging scaffolding was constructed and fifteen horizontal drillings up to 9 m in depth were conducted, where the still anchors were fixed and cemented (Figure 19c). The integrity of the rock surface was restored, leaving no visual effects. A water-drainage structure will be also planned in correspondence to the ephemeral stream highlighted in Figure 16c. This first stage of mitigation works will allow the opening of the historical entrance into the Uplistsikhe rock town, located at the bottom of the rock cliff.

5.2.4. The Monastery of Petra

As confirmed by IRT surveys and the field inspections the water seepage in the rock mass occurs not from single points but is generally diffused along an alignment connected to the bedding, below which the rock mass is probably fully saturated. This is in agreement with the hypothesis of [44], which states that the seepage detected in 2014 (Figures 5b,c and 17) is probably the result of the rock mass water circulation from a back-side reservoir (as shown by the dampness of the rock mass), where a dam was recently constructed in a gorge passing on the left side of the monument and a nearby old Nabatean cistern [88]. The increase of seepage from 2011 to 2014 can be likely related to the exceptional rainfall occurring from December 2013 to March 2014 (Figure 20), that may have produced the storage inside the nearby cistern or relevant seepage in the rock mass [89]. Ref. [42] identifies another possible cause for the seepage in a mixed influence of the dam and rainfall. Nevertheless, the relationship between seepage vs. rainfall, cisterns, and the recently realized reservoir with the construction of a dam, should be better investigated. Other cisterns are also present in the same area [89] but, according to [44], they do not play a major role in water seepage in the monastery. The performed analysis suggests the need to mitigate the impact of rising dampness (especially along the monastery left side basement) and to verify the potential weathering of the rock also in terms of geomechanical strength reduction.
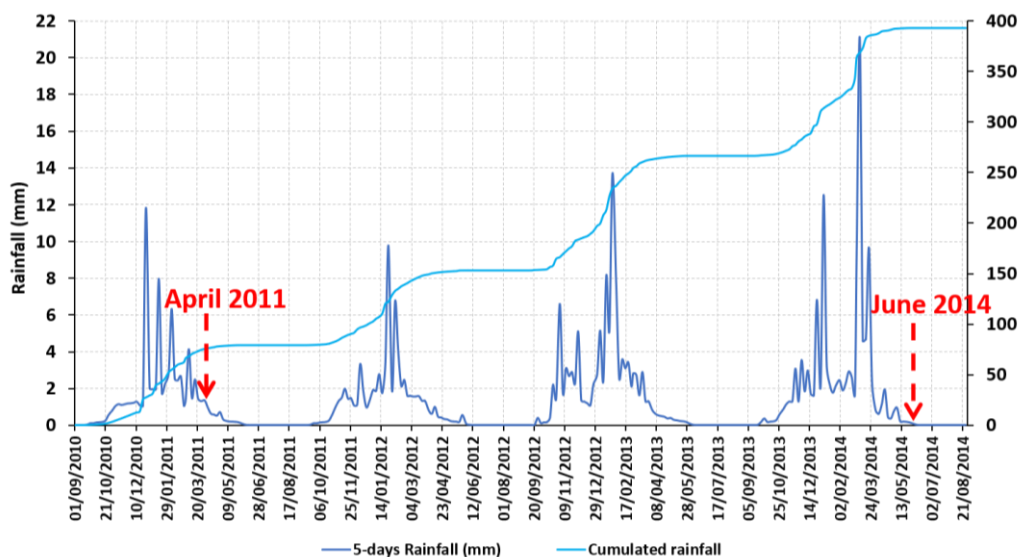

Figure 20. Rainfall data in Petra between September 2010 and 2014 [90].

5.3. IRT and UAV-DP for Protection/Conservation Strategies of Rupestrian Cultural Heritage

Protecting rupestrian cultural heritage from weathering, erosion, and slope instability using advanced RS techniques is a fundamental step towards a sustainable conservation strategy, especially when traditional knowledge is being progressively abandoned and/or forgotten [16]. In the protection and conservation of the investigated sites, the

applied integration of close-range remote sensing techniques provided a versatile ancillary low-cost tool for identifying the main critical sectors of the analyzed sites by means of a rapid morpho-structural and hydrographic characterization. In particular IRT was used to integrate field surveys for remote geomechanical surveying of aperture and seepage parameters and to confirm the ephemeral drainage network patterns obtained by performing the hydromodelling on the UAV-DP 3D models. These latter were also combined with the field collected structural data to obtain a 3D kinematic analysis for identifying the main instability phenomena and mapping their spatial probability of occurrence on the rock slopes. One of the limits of the graphic kinematic analysis is that of considering an infinite persistence, zero friction angle, not taking into account the variability of the parameters that determine the friction angle; in fact, the roughness, the uniaxial compression strength and the eventual filling of the discontinuities differ according to the fractures. These are identified by combining fracture dip and dip directions with the local slope orientations. The adopted methodology can rapidly and successfully lead to identifying the presence of conservation criticalities such as moisture zones connected to surface water runoff/concentration areas, ephemeral drainage networks, ground water seepage, open fractures, and potentially unstable ledge-niche systems. In the case studies of Georgia large areas of the slope surface were inaccessible; therefore, the remote sensing approach provided a time-effective mapping while granting the safety of operators. The adopted remote sensing techniques are not time consuming (all the surveys were carried out in one working day, as well as the data processing), have relative low cost and grant a nondestructive approach for the safety of both the monument and the operator. Nevertheless, field surveys are still necessary to collect geomechanical and geotechnical parameters and collect samples for laboratory analysis.

6. Conclusions

The present paper describes the support activities for rupestrian cultural heritage protection and conservation activities carried out in Georgia and in Petra (Jordan) between 2014 and 2018. Different rupestrian monasteries carved in weak rocks were surveyed by means of traditional surveys and close-range nondestructive remote sensing techniques, such as IRT and UAV-DP, in order to collect geomechanical parameters, perform preliminary landslide hazard assessment and identify the main conservation problems, with the final aim of defining preliminary sustainable mitigation measures. In particular, IRT and UAV-DP were integrated to provide an accurate slope-scale mapping of potential criticalities with respect to weathering and degradation and slope instability, such as water runoff concentration areas, moisture/seepage sectors, and open fractures. 3D kinematic analysis was also performed to detect the areas characterized by higher susceptibility with respect to the different instability phenomena. Field surveys and geotechnical analysis were carried out to validate the outcomes of the RS activity and improve the geotechnical characterization of the sites. Sustainable preservation of rupestrian cultural heritage sites carved in weak rocks such as tuffs and soft sandstones depends on several natural factors, among which the most important are avoiding surface runoff, -ground water infiltration, sealing open fractures, and reinforcing ledge-niche systems. Reducing surface water interaction is also fundamental so as to preserve unique mural paintings and wall inscriptions. Nevertheless, only a multidisciplinary approach can define a new paradigm for protection and conservation strategies of rupestrian cultural heritage sites: understanding the ongoing weathering/erosion phenomena as well as the instability processes is the main target in order to define a general master plan of sustainable mitigation measures and choose the most suitable monitoring system. The performed method can be used in similar geological contexts where the areas at risk are vulnerable and hardly accessible even for professional rock climbers.

Author Contributions: W.F. conceived the article structure, collected, processed, and analyzed the IRT data in Georgia; M.E. supervised the Georgian team and provided insights on the mitigation strategies; D.S., and G.G. performed the field surveys, provided structural-geotechnical data and

References

1. Sdao, F.; Lioi, D.S.; Pascale, S.; Caniani, D.; Mancini, I.M. Landslide susceptibility assessment by using a neuro-fuzzy model: A case study in the Rupestrian heritage rich area of Matera. *Nat. Hazards Earth Syst. Sci.* **2013**, *13*, 395–407. [CrossRef]
2. Taboroff, J. Cultural heritage and natural disasters: Incentives for risk management and mitigation. In *Managing Disaster Risk in Emerging Economies*; Kreimer, A., Arnold, M., Eds.; World Bank Publications, Disaster Management Risk: New York, NY, USA, 2000; Volume 2, pp. 71–79.
3. Wang, J.J. Flood risk maps to cultural heritage: Measures and process. *J. Cult. Herit.* **2015**, *16*, 210–220. [CrossRef]
4. Sileo, M.; Gizzi, F.T.; Donvito, A.; Lasaponara, R.; Fiore, F.; Masini, N. Multi-Scale Monitoring of Rupestrian Heritage: Method-ological Approach and Application to a Case Study. *Int. J. Archit. Herit.* **2020**, 1–16. [CrossRef]
5. Timothy, P.W.; Stratulat, A.; Duffus, P.; Pre'vost, J.H.; George, W.; Scherer, W.G. Flaw propagation and buckling in clay-bearing sandstones. *Environ. Geol.* **2011**, *63*, 1565–1572.
6. Banerjee, N.R.; Muehlenbachs, K. Tuff life: Bioalteration in volcaniclastic rocks from the Ontong Java Plateau. *Geochem. Geophys. Geosystems* **2003**, *4*. [CrossRef]
7. Wedekind, W.; López-Doncel, R.; Dohrmann, R.; Kocher, M.; Siegesmund, S. Weathering of volcanic tuff rocks caused by moisture expansion. *Environ. Earth Sci.* **2013**, *69*, 1203–1224. [CrossRef]
8. Ruedrich, J.; Bartelsen, T.; Dohrmann, R.; Siegesmund, S. Moisture expansion as a deterioration factor for sandstone used in buildings. *Environ. Earth Sci.* **2011**, *63*, 1545–1564. [CrossRef]
9. Weiss, T.; Siegesmund, S.; Kirchner, D.; Sippel, J. Insulation weathering and hygric dilatation as a control on building stone degradation. *Environ. Geol.* **2004**, *46*, 402–413. [CrossRef]

10. Topal, T.; Doyuran, V. Engineering geological properties and durability assessment of the Cappadocian tuff. *Eng. Geol.* **1997**, *47*, 175–187. [CrossRef]

11. Boldini, D.; Guido, G.L.; Margottini, C.; Spizzichino, D. Stability analysis of a large-volume block in the historical rock-cut city of Vardzia (Georgia). *Rock Mech. Rock Eng.* **2018**, *51*, 341–349. [CrossRef]

12. ISRM. Suggested methods for the quantitative description of discontinuities in rock masses. *Int. J. Rock Mech. Min. Sci. Geomech. Abstr.* **1978**, *15*, 319–368.

13. Frodella, W.; Elashvili, M.; Spizzichino, D.; Gigli, G.; Adikashvili, L.; Vacheishvili, N.; Kirkitadze, G.; Nadaraia, A.; Margottini, C.; Casagli, N. Combining InfraRed Thermography and UAV Digital Photogrammetry for the Protection and Conservation of Rupestrian Cultural Heritage Sites in Georgia: A Methodological Application. *Remote Sens.* **2020**, *12*, 892. [CrossRef]

14. Marszałek, M.; Alexandrowicz, Z.; Rzepa, G. Composition of weathering crusts on sandstones from natural outcrops and architectonic elements in an urban environment. *Environ. Sci. Pollut. Res.* **2014**, *21*, 14023–14036. [CrossRef]

15. Pecchioni, E.; Vettori, S.; Cantisani, E.; Fratini, F.; Ricci, M.; Garzonio, C.A. Chemical and mineralogical studies of the red chromatic alteration of Florentine Pietra Serena sandstone. *Eur. J. Mineral.* **2016**, *28*, 449–458. [CrossRef]

16. Margottini, C.; Gigli, G.; Ruther, H.; Spizzichino, D. Advances in Geotechnical Investigations and Monitoring in Rupestrian Settlements Inscribed in the UNESCO's World Heritage List. *Procedia Earth Planet. Sci.* **2016**, *16*, 35–51. [CrossRef]

17. Tunusluoglu, M.C.; Zorlu, K. Rockfall hazard assessment in a cultural and natural heritage (Ortahisar Castle, Cappadocia, Turkey). *Environ. Geol.* **2009**, *56*, 963–972. [CrossRef]

18. UNESCO World Heritage List. Available online: https://whc.unesco.org/en/list (accessed on 21 January 2021).

19. UNESCO Tentative List. Available online: https://whc.unesco.org/en/tentativelists (accessed on 21 January 2021).

20. Margottini, C.; Antidze, N.; Corominas, J.; Crosta, G.B.; Frattini, P.; Gigli, G.; Giordan, D.; Iwasaky, I.; Lollino, G.; Manconi, A.; et al. Landslide hazard, monitoring and conservation strategy for the safeguard of Vardzia Byzantine monastery complex, Georgia. *Landslides* **2015**, *12*, 193–204. [CrossRef]

21. Nikolakopoulos, K.; Kavoura, K.; Depountis, N.; Kyriou, A.; Argyropoulos, N.; Koukouvelas, I.; Sabatakakis, N. Preliminary results from active landslide monitoring using multidisciplinary surveys. *Eur. J. Remote Sens.* **2017**, *50*, 280–299. [CrossRef]

22. Frodella, W.; Ciampalini, A.; Gigli, G.; Lombardi, L.; Raspini, F.; Nocentini, M.; Scardigli, C.; Casagli, N. Synergic use of satellite and ground based remote sensing methods for monitoring the San Leo rock cliff (Northern Italy). *Geomorphology* **2016**, *264*, 80–94. [CrossRef]

23. Spizzichino, D.; Boldini, D.; Frodella, W.; Elashvili, M.; Margottini, C. Landslide risk analysis and mitigation for the ancient rock-cut city of Vardzia (Georgia). In *Proceedings of 2017 IPL Symposium*; UNESCO: Paris, France, 2017; pp. 1–8.

24. Frodella, W.; Spizzichino, D.; Gigli, G.; Elashvili, M.; Margottini, C.; Villa, A.; Frattini, P.; Crosta, G.; Casagli, N. Integrating Kinematic Analysis and Infrared Thermography for Instability Processes Assessment in the Rupestrian Monastery Complex of David Gareja (Georgia). In *Understanding and Reducing Landslide Disaster Risk*; Springer: Cham, Germany, 2020; pp. 457–463.

25. David Gareji Monasteries and Hermitages, Georgia Technical Report, The 7 Most Endangered, Europa Nostra. Campbell. 2018. Available online: https://www.europanostra.org/wp-content/uploads/2019/10/7ME-2019-Georgia-DavidGarejiMonasteries-Report.pdf (accessed on 29 January 2021).

26. UNESCO World Heritage List, Petra. Available online: https://whc.unesco.org/en/list/326 (accessed on 21 January 2021).

27. Lebedev, V.A.; Chernyshev, I.V.; Vashakidze, G.T.; Gudina, M.V.; Yakushev, A.I. Geochronology of Miocene volcanism in the northern part of the Lesser Caucasus (Erusheti Highland, Georgia). In *Doklady Earth Sciences*; Springer Science & Business Media: Berlin, Germany, 2012; Volume 444, p. 585. Available online: https://www.researchgate.net/profile/V-Lebedev-3/publication/257850126_Geochronology_of_miocene_volcanism_in_the_northern_part_of_the_Lesser_Caucasus_Erusheti_Highland_Georgia/links/00463528ef324cb0a1000000/Geochronology-of-miocene-volcanism-in-the-northern-part-of-the-Lesser-Caucasus-Erusheti-Highland-Georgia.pdf (accessed on 29 January 2021).

28. Okrostsvaridze, A.; Popkhadze, N.; Bluashvili, D.; Chang, Y.H.; Skhirtladze, I. Pliocene Quaternary Samtskhe-Javakheti Volcanic Highland, Lesser Caucasus—as a result of mantle plumes activity. In *Proceedings of the Fourth Plenary Conference of IGCP 610 From the Caspian to Mediterranean: Environmental Change and Human Response during the Quaternary, Tbilisi, Georgia, 2–9 October 2016*; Gilbert, A.S., Yanko-Hombach, V., Eds.; Georgian National Academy of Sciences: Tbilisi, Georgia, 2016; pp. 127–131.

29. Okrostsvaridze, A.; Chung, S.L.; Lin, Y.C.; Skhirtladze, I. Geology and zircon U-Pb geochronology of the Mtkvari pyroclastic flow and evaluation of destructive processes affecting Vardzia rock-cut city, Georgia. *Quat. Int.* **2020**, *540*, 137–145. [CrossRef]

30. Okrostsvaridze, A.; Elashvili, M.; Nino Popkhadze, N.; Kirkitadze, G. New Data on the Geological Structure of the Vardzia Cave City, Georgia. *Bull. Georgian Natl. Acad. Sci.* **2016**, *10*, 98–106.

31. Okrostsvaridze, A.; Gagnidze, N.; Bobrova, I.; Skhirtladze, I. Late Miocene volcanic ash layers of the intermountain depression of the eastern Caucasus: The product of a megacaldera explosion? In Proceedings of the Joint meeting of IGCP 610 and INQUA POCAS Focus Group, Palermo, Italy, 1–9 October 2017.

32. Okrostsvaridze, A.; Popkhadze, N. Megavolcano in the Late Cenozoic Samtckhe Javakheti Volcanic Province? Lesser Caucasus, Georgia-Turkish Border. In *Proceedings of the VI International Workshop on Collapse Calderas, Hokkaido, Japan, 4–10 September 2016*; International Association of Volcanology and Chemistry of the Earth's Interior: Rome, Italy, 2016; p. 42. Available online: http://eprints.iliauni.edu.ge/6373/ (accessed on 29 January 2021).

33. Gamkrelidze, I.; Okrostsvaridze, A.; Gagnidze, N. Field trip guide of the fourth plenary conference. In Proceedings of the IGCP 610 "From the Caspian to Mediterranean: Environmental Change and Human Response during the Quaternary" (2013–2017), Fourth Plenary Conference and Field Trip, Tbilisi, Georgia, 2–9 October 2016.

34. Margottini, C.; Spizzichino, D.; Gigli, G.; Frodella, W.; Elashvili, M.; Alberti, S.; Valagussa, A.; Crosta, G. Instability processes affecting the rupestrian monastery complex area of Davit Gareja (Georgia). In Proceedings of the International Conference: Davit Gareji, Multidisciplinary Study and Development Strategy, Tbilisi, Georgia, 18–20 April 2020; pp. 187–193. Available online: https://www.researchgate.net/profile/William-Frodella/publication/332013627_Instability_processes_affecting_the_rupestrian_monastery_complex_area_of_David_Gareja_Georgia/links/5f0f0415299bf1e548b71490/Instability-processes-affecting-the-rupestrian-monastery-complex-area-of-David-Gareja-Georgia.pdf (accessed on 29 January 2021).

35. UNESCO Tentative List, David Gareja. Available online: https://whc.unesco.org/en/tentativelists/5224 (accessed on 21 January 2021).

36. Stinghen, A. Tectonic and Geomorphological Evolution of the Kartalini Basin, Georgia. Master's thesis, University of Padua, Padova PD, Italy, 2011; 109p.

37. Khimshiashvili, K. The architecture of Uphlistsikhe, Georgia. *Trans. Anc. Monum. Soc.* **1999**, 77–100.

38. ICOMOS. World Report on Monuments and Sites in Danger Georgia. 2001. Available online: https://www.icomos.org/risk/2001/geor2001.htm (accessed on 4 January 2021).

39. UNESCO World Heritage List, Uplistsikhe. Available online: https://whc.unesco.org/en/tentativelists/5234 (accessed on 21 January 2021).

40. Alshawabkeh, Y.; Bal'awi, F.; Haala, N. 3D Digital Documentation, Assessment, and Damage Quantification of the Al-Deir Monument in the Ancient City of Petra, Jordan. *Conserv. Manag. Archaeol. Sites* **2010**, *12*, 124–145. [CrossRef]

41. Margottini, C.; Spizzichino, D. Historical accesses to UNESCO cultural heritages: Engineering geology for the sustainable conservation of Petra Siq. *Innov. Infrastruct. Solut.* **2017**, *2*, 25. [CrossRef]

42. Barjous, M.O.; Jaser, D. Geotechnical Studies and Geological Mapping of Ancient Petra City. Amman: The Hashemite Kingdom of Jordan, Ministry of Energy and Mineral Resources, Natural Resources Authority, Geology Directorate, Geological Mapping Division. 1992. Available online: https://pascal-francis.inist.fr/vibad/index.php?action=getRecordDetail&idt=6402229 (accessed on 29 January 2021).

43. Bumbaru, D.; Burke, S.; Petzet, M.; Truscott, M.; Ziesemer, J. *Jordan Heritage @ Risk! In Heritage at Risk, ICOMOS World Report 2000 on Monuments and Sites in Danger*; ICOMOS: Munich, Germany, 2000; pp. 123–124.

44. Chambel, A.; Colvin, C. A geological and hydrogeological assessment of "El Dir" monastery, Petra (Jordan). UNESCO Unpublished Report. 23 September 2010.

45. Rocscience, Dips. *v8 Graphical and Statistical Analysis of Orientation Data*; Rocscience Inc.: Toronto, ON, Canada, 2020.

46. ISRM Suggested methods for determining point load strength. *Int. J. Rock Mech. Min. Sci. Geomech.* **1985**, *22*, 51–62. [CrossRef]

47. Teza, G.; Marcato, G.; Castelli, E.; Galgaro, A. IRTROCK: A matlab toolbox for contactless recognition of surface and shallow weakness traces of a rock mass by infrared thermography. *Comput. Geosci.* **2012**, *45*, 109–118. [CrossRef]

48. Maldague, X. *Theory and Practice of Infrared Technology for Non-Destructive Testing*; John-Wiley & Sons: Hoboken, NJ, USA, 2001; 684p.

49. Spampinato, L.; Calvari, S.; Oppenheimer, C.; Boschi, E. Volcano surveillance using infrared cameras. *Earth-Sci. Rev.* **2011**, *106*, 63–91. [CrossRef]

50. Avdelidis, N.P.; Moropoulou, A.; Theoulakis, P. Detection of water deposits and movement in porous materials by infrared imaging. *Infrared Phys. Technol.* **2003**, *44*, 183–190. [CrossRef]

51. Tavukçuoğlu, A.; Dügünes, E.N.; Caner-Saltık, Ş.; Demirci, A. Use of IR thermography for the assessment of surface-water drainage problems in a historical building, Ağzıkara-han (Aksaray), Turkey. *NDT E Int.* **2005**, *38*, 402–410. [CrossRef]

52. Aggelis, D.G.; Kordatos, E.Z.; Soulioti, D.V.; Matikas, T.E. Combined use of thermography and ultrasound for the characterization of subsurface cracks in concrete. *Constr. Build. Mater.* **2010**, *24*, 1888–1897. [CrossRef]

53. De Freitas, S.S.; De Freitas, V.P.; Barreira, E. Detection of façade plaster detach-ments using infrared thermography, a nondestructive technique. *Constr. Build. Mater.* **2014**, *70*, 80–87. [CrossRef]

54. Cabrelles, M.; Galcerá, S.; Navarro, S.; Lerma, J.L.; Akasheh, T.; Haddad, N. Integration of 3D laser scanning, photogrammetry and thermography to record architectural monuments. In Proceedings of the 22nd CIPA Symposium, Kyoto, Japan, 11–15 October 2009.

55. Frodella, W.; Gigli, G.; Morelli, S.; Lombardi, L.; Casagli, N. Landslide Mapping and Characterization through Infrared Thermography (IRT): Suggestions for a Methodological Approach from Some Case Studies. *Remote Sens.* **2017**, *9*, 1281. [CrossRef]

56. Gigli, G.; Frodella, W.; Garfagnoli, F.; Morelli, S.; Mugnai, F.; Menna, F.; Casagli, N. 3-D geomechanical rock mass characterization for the evaluation of rockslide susceptibility scenarios. *Landslides* **2014**, *11*, 131–140. [CrossRef]

57. Pappalardo, G.; Mineo, S.; Imposa, S.; Grassi, S.; Leotta, A.; La Rosa, F.; Salerno, D. A quick combined approach for the characterization of a cliff during a post-rockfall emergency. *Landslides* **2020**, *17*, 1063–1081. [CrossRef]

58. Frodella, W.; Morelli, S.; Pazzi, V. Infrared Thermographic surveys for landslide mapping and characterization: The Rotolon DSGSD (Norther Italy) case study. *Ital. J. Eng. Geol. Environ.* **2017**, *2017*, 77–84.

59. Di Traglia, F.; Nolesini, T.; Solari, L.; Ciampalini, A.; Frodella, W.; Steri, D.; Allotta, B.; Rindi, A.; Marini, L.; Monni, N.; et al. Lava delta deformation as a proxy for submarine slope instability. *Earth Planet. Sci. Lett.* **2018**, *488*, 46–58. [CrossRef]

60. FLIR Systems Inc. FLIR ThermaCAM SC620 technical specifications. 2009. Available online: www.flir.com/cs/emea/en/view/?id=41965 (accessed on 31 July 2019).

61. FLIR Systems Inc. FLIR ThermaCAM B425. 2009. Available online: http://www.thermalimagingcamera.co.uk/media/downloads/14/flir-b425-ir-camera-datasheet.pdf (accessed on 31 December 2020).
62. FLIR Systems Inc. FLIR Tools+ Datasheet. 2015. Available online: https://www.infraredcamerawarehouse.com/content/FLIR%20Datasheets/FLIR%20ToolsPlus%20Datasheet.pdf (accessed on 30 September 2019).
63. ESRI Inc. ArcMap 10.6 Datasheet. 2019. Available online: https://www.esri.com/content/dam/esrisites/en-us/media/pdf/product/desktop/ArcGIS-10.6-Desktop-ArcMap-Functionality-Matrix.pdf (accessed on 31 October 2019).
64. Chandler, J. Effective application of automated digital photogrammetry for geomorphological research. *Earth Surf. Process Landf.* **1999**, *24*, 51–63. [CrossRef]
65. Zhang, Z.; Zheng, S.; Zhan, Z. Digital terrestrial photogrammetry with photo total station. *Int. Arch. Photogramm. Remote Sens.* **2004**, 232–236. Available online: https://citeseerx.ist.psu.edu/viewdoc/download?doi=10.1.1.58.7457&rep=rep1&type=pdf (accessed on 29 January 2021).
66. Grün, A.; Remondino, F.; Zhang, L. Reconstruction of the Great Buddha of Bamiyan, Afghanistan. *Int. Arch. Photogramm. Remote Sens.* **2002**, *34*, 363–368.
67. Rinaudo, F.; Chiabrando, F.; Lingua, A.; Spanò, A. Archaeological site monitoring: UAV photogrammetry can be an answer. International Archives of the Photogrammetry. *Remote Sens. Spat. Inf. Sci.* **2012**, *39*, 583–588.
68. Remondino, F.; Barazzetti, L.; Nex, F.; Scaioni, M.; Sarazzi, D. UAV photogrammetry for mapping and 3d modeling–current status and future perspectives. International archives of the photogrammetry. *Remote Sens. Spat. Inf. Sci.* **2011**, *38*, C22.
69. Bolognesi, M.; Furini, A.; Russo, V.; Pellegrinelli, A.; Russo, P. Accuracy of cultural heritage 3D models by RPAS and terrestrial photogrammetry. The International Archives of Photogrammetry. *Remote Sens. Spat. Inf. Sci.* **2014**, *40*, 113.
70. Agisoft Photoscan, Datasheet. 2017. Available online: https://www.agisoft.com/pdf/photoscan-pro_1_4_en.pdf (accessed on 31 December 2020).
71. Riegl VZ-400 Datasheet. 2017. Available online: www.riegl.com/uploads/tx_pxpriegldownloads/10_DataSheet_VZ-400_2017-06-14.pdf (accessed on 31 December 2020).
72. Hoek, E.; Bray, J.W. *Rock Slope Engineering*, 3rd ed.; Institute of Mining and Metallurgy: London, UK, 1981.
73. Goodman, R.E.; Bray, J.W. Toppling of rock slopes. In Proceedings of the ASCE Specialty Conference on Rock Engineering for Foundations and Slopes, Boulder, CO, USA, 15–18 August 1976; Volume 2, pp. 201–234. Available online: https://ci.nii.ac.jp/naid/10004542689/ (accessed on 29 January 2021).
74. Hudson, J.A.; Harrison, J.P. *Engineering Rock Mechanics*; Pergamon Press: Oxford, UK, 1997; p. 444.
75. Casagli, N.; Pini, G. Analisi cinematica della stabilità di versanti naturali e fronti di scavo in roccia. *Geol. Appl. E Idrogeol.* **1993**, *28*, 223–232. (In Italian)
76. Lombardi, L. Nuove Tecnologie di Rilevamento e di Analisi di Dati Goemeccanici per la Valutazione della Sicurezza. Unpublished Ph.D. Thesis, University of Florence, Piazza di San Marco, Firenze, Italy, 2007. (In Italian).
77. Gigli, G.; Frodella, W.; Mugnai, F.; Tapete, D.; Cigna, F.; Fanti, R.; Intrieri, E.; Lombardi, L. Instability mechanisms affecting cultural heritage sites in the Maltese Archipelago. *Nat. Hazards Earth Syst. Sci.* **2012**, *12*, 1–21. [CrossRef]
78. Gigli, G.; Casagli, N. Semi-automatic extraction of rock mass structural data from high resolution LIDAR point clouds. *Int. J. Rock Mech. Min. Sci.* **2011**, *48*, 187–198. [CrossRef]
79. DGM, AB, RM (2015) CloudCompare-User's Manual for version 2.6.1. Available online: https://www.danielgm.net/cc/doc/qCC/CloudCompare%20v2.6.1%20-%20User%20manual.pdf (accessed on 21 December 2020).
80. Boldini, D.; Wang, F.; Sassa, K.; Tommasi, P. Mechanism of landslide causing the December 2002 tsunami at Stromboli volcano (Italy). In *Landslides*; Springer: Berlin/Heidelberg, Germany, 2005; pp. 173–180.
81. Rotonda, T.; Tommasi, P.; Boldini, D. Geomechanical characterization of the volcaniclastic material involved in the 2002 landslides at Stromboli. *J. Geotech. Geoenvironmental Eng.* **2009**, *136*, 389–401. [CrossRef]
82. Spizzichino, D.; Margottini, C. *Evidences on the Groundwater seepage nearby the monument "El Deir" or "Monastery", at the ancient city of Petra*; Internal Report; Superior Institute for Protection and Environmental Research (ISPRA): Rome, Italy, 2014.
83. Dixon, J.B.; Weed, S.B. *Minerals in Soil Environments*, 2nd ed.; Soil Science Society of America: Madison, WI, USA, 1989; p. 1244.
84. Heinrichs, K. Diagnosis of Weathering Damage on Rock-Cut Monuments in Petra, Jordan. *Environ. Geol.* **2008**, *56*, 643–675. [CrossRef]
85. Nichols, G. *Sedimentology and Stratigraphy*, 2nd ed.; Wiley-Blackwell: Oxford, UK, 2009.
86. Verezen, V.A.M. The Crumbling Wonder: A damage-and risk-assessment of sandstone monuments and natural features in the Petra Archaeological Park (Jordan). *Int. J. Stud. Res. Archaeol.* **2017**, *3*, 20–34.
87. Eklund, S. Stone Weathering in the Monastic Building Complex on Mountain of St Aaron in Petra, Jordan. Unpublished Master's Thesis, University of Helsinki, Department of Archaeology, Helsinki, Finland, 2008. Available online: https://oa.doria.fi/bitstream/handle/10024/43682/stonewea.pdf?sequence=1 (accessed on 8 December 2020).
88. Ortloff, C.R. The Water Supply and Distribution System of the Nabataean City of Petra (Jordan), 300 BC–AD 300. *Camb. Archaeol. J.* **2005**, *15*, 93–109. [CrossRef]
89. US-ICOMOS Jordan. *US-ICOMOS Management Analysis and Recommendations for the Petra World Heritage Site*; Report; US-ICOMOS: Amman, Jordan, 1996.
90. Climate Engine. Available online: https://clim-engine-development.appspot.com (accessed on 20 January 2021).